OPEN ACCESS

ORIGINAL RESEARCH

Mitochondrial dysfunction during loss of prohibitin 1 triggers Paneth cell defects and ileitis

Dakota N Jackson,[1] Marina Panopoulos,[1] William L Neumann,[2] Kevin Turner,[3] Brandi L Cantarel,[3] LuAnn Thompson-Snipes,[1] Themistocles Dassopoulos ,[1] Linda A Feagins,[4] Rhonda F Souza ,[5] Jason C Mills,[6] Richard S Blumberg,[7] K Venuprasad,[3] Winston E Thompson,[8] Arianne L Theiss [1]

► Additional material is published online only. To view please visit the journal online (http://dx.doi.org/10.1136/gutjnl-2019-319523).

For numbered affiliations see end of article.

Correspondence to
Dr Arianne L Theiss, Baylor Scott and White Research Institute, Dallas, TX 75204, USA; arianne.theiss@cuanschutz.edu

Received 23 July 2019
Revised 24 January 2020
Accepted 3 February 2020

ABSTRACT

Objective Although perturbations in mitochondrial function and structure have been described in the intestinal epithelium of Crohn's disease and ulcerative colitis patients, the role of epithelial mitochondrial stress in the pathophysiology of inflammatory bowel diseases (IBD) is not well elucidated. Prohibitin 1 (PHB1), a major component protein of the inner mitochondrial membrane crucial for optimal respiratory chain assembly and function, is decreased during IBD.

Design Male and female mice with inducible intestinal epithelial cell deletion of *Phb1* (*Phb1*$^{i\Delta IEC}$) or Paneth cell-specific deletion of *Phb1* (*Phb1*$^{\Delta PC}$) and *Phb1*$^{fl/fl}$ control mice were housed up to 20 weeks to characterise the impact of PHB1 deletion on intestinal homeostasis. To suppress mitochondrial reactive oxygen species, a mitochondrial-targeted antioxidant, Mito-Tempo, was administered. To examine epithelial cell-intrinsic responses, intestinal enteroids were generated from crypts of *Phb1*$^{i\Delta IEC}$ or *Phb1*$^{\Delta PC}$ mice.

Results *Phb1*$^{i\Delta IEC}$ mice exhibited spontaneous ileal inflammation that was preceded by mitochondrial dysfunction in all IECs and early abnormalities in Paneth cells. Mito-Tempo ameliorated mitochondrial dysfunction, Paneth cell abnormalities and ileitis in *Phb1*$^{i\Delta IEC}$ ileum. Deletion of *Phb1* specifically in Paneth cells (*Phb1*$^{\Delta PC}$) was sufficient to cause ileitis. Intestinal enteroids generated from crypts of *Phb1*$^{i\Delta IEC}$ or *Phb1*$^{\Delta PC}$ mice exhibited decreased viability and Paneth cell defects that were improved by Mito-Tempo.

Conclusion Our results identify Paneth cells as highly susceptible to mitochondrial dysfunction and central to the pathogenesis of ileitis, with translational implications for the subset of Crohn's disease patients exhibiting Paneth cell defects.

Significance of this study

What is already known on this subject?

- Previous studies suggest the involvement of epithelial mitochondrial dysfunction in the pathophysiology of inflammatory bowel disease, including Crohn's disease and ulcerative colitis.

What are the new findings?

- We identify Paneth cells as highly susceptible to mitochondrial dysfunction driven by Prohibitin 1 (*Phb1*) deletion and central to the development of ileitis.
- Treatment of Paneth cell defects with Mito-Tempo during *Phb1* deletion implicates a potential therapeutic application for abnormal Paneth cells via elimination of mitochondrial-derived reactive oxygen species.
- Mito-Tempo also prevented the upregulation of interleukin-1β (IL-1β) and IL-18 in the ileum that were induced early after *Phb1* deletion.
- *Phb1* deficiency induced loss of viability of the intestinal stem cell niche and Paneth cell defects in cultured enteroids.

How might it impact on clinical practice in the foreseeable future?

- These are the first results that present a causative role of mitochondrial dysfunction in ileitis that initiates in Paneth cells.
- Mitochondrial-targeted therapeutics may have translational utility in a subset of Crohn's disease patients exhibiting Paneth cell defects.

INTRODUCTION

Crohn's disease, an inflammatory bowel disease (IBD) characterised by recurring, incurable, chronic inflammation, is considered a global health problem with accelerating incidence in newly industrialized countries and stabilising, yet high prevalence in Western countries.[1] Crohn's disease is a multifactorial disease exhibiting loss of intestinal epithelial cell (IEC) barrier integrity and dysregulated immune cell responses due to unknown environmental triggers in genetically predisposed individuals.[2] Genome-wide association studies have identified ~200 IBD risk loci,[3] with 5% of these genes functionally linked to the maintenance of mitochondrial health.[4] Mitochondria are dynamic organelles that readily respond to environmental stimuli and cellular demands for energy. Mitochondria are coordinators of cellular homoeostasis via their role in energy production and oxidative metabolism, induction of apoptosis, regulation of calcium, production of reactive oxygen species (ROS), and regulation of signal transduction and epigenomic intermediates. In the intestine, mitochondrial metabolism and function play key roles

Linked

► http://dx.doi.org/10.1136/gutjnl-2019-319514

Check for updates

To cite: Jackson DN, Panopoulos M, Neumann WL, *et al*. *Gut* Epub ahead of print: [*please include* Day Month Year]. doi:10.1136/gutjnl-2019-319523

in immune cell activation, IEC barrier integrity and IEC differentiation programmes and stemness.[5 6] Previous studies suggest the involvement of epithelial mitochondrial dysfunction in the pathophysiology of IBD, including Crohn's disease and ulcerative colitis,[7 8] but whether this is a cause or consequence of the pathogenesis of IBD is not known.

Prohibitin 1 (PHB1) belongs to a family of proteins that share an evolutionarily conserved stomatin/prohibitin/flotillin/HflK/C domain and serves diverse roles in cell function including regulation of cell cycle progression, apoptosis and transcription depending on its subcellular localisation. In IECs, PHB1 predominantly localises to the mitochondria.[9] PHB1 is the major component protein of the inner mitochondrial membrane (IMM) where it forms a heterodimeric complex with PHB2 to exert chaperon function to stabilise mitochondrial DNA (mtDNA)-encoded proteins and regulate optic atrophy 1 (OPA1)-dependent IMM fusion.[10] Additionally, PHB1 interacts with and is required for optimal activity of complexes I and IV of the electron transport chain (ETC).[10] Expression of PHB1 is decreased in mucosal biopsies from IBD-afflicted patients.[9 11] We previously showed that overexpression of epithelial PHB1 using genetic manipulation (*Villin-Phb1* transgenic mice) or therapeutic delivery to the colon decreases oxidative stress and protects mice from experimental colitis.[12 13] Given the known functions of PHB1 in mitochondrial structure and dynamics, we generated three novel mouse models of mitochondrial dysfunction via *Phb1* deletion in the intestinal epithelium or specifically in Paneth cells. Here, we investigated the role of IEC mitochondrial dysfunction in intestinal inflammation.

RESULTS

Phb1$^{i\Delta IEC}$ mice develop spontaneous ileitis

Genetic deletion of *Phb1* results in embryonic lethality in mice and flies.[14] To gain tissue and temporal control of PHB1 deletion, we ablated PHB1 in IECs of adult *Phb1* floxed mice (*Phb1*$^{fl/fl}$*:Villin*-CreERT2 referred to as *Phb1*$^{i\Delta IEC}$ mice) by tamoxifen administration. The absence of PHB1 protein in the epithelium was confirmed by western immunoblotting and immunohistochemistry (IHC) staining after tamoxifen injection (online supplementary figure S1). Beginning at 7 weeks after induction of *Phb1* deletion, *Phb1*$^{i\Delta IEC}$ mice gained less body weight compared with *Phb1*$^{fl/fl}$ littermates (online supplementary figure S2A). Within 12 weeks after induction of *Phb1* deletion, *Phb1*$^{i\Delta IEC}$ mice manifested spontaneous, discontinuous ileal inflammation (figure 1A), while sparing more proximal small intestine and colon (online supplementary figure S2B). Histological alterations in the ileum included infiltration of immune cells,

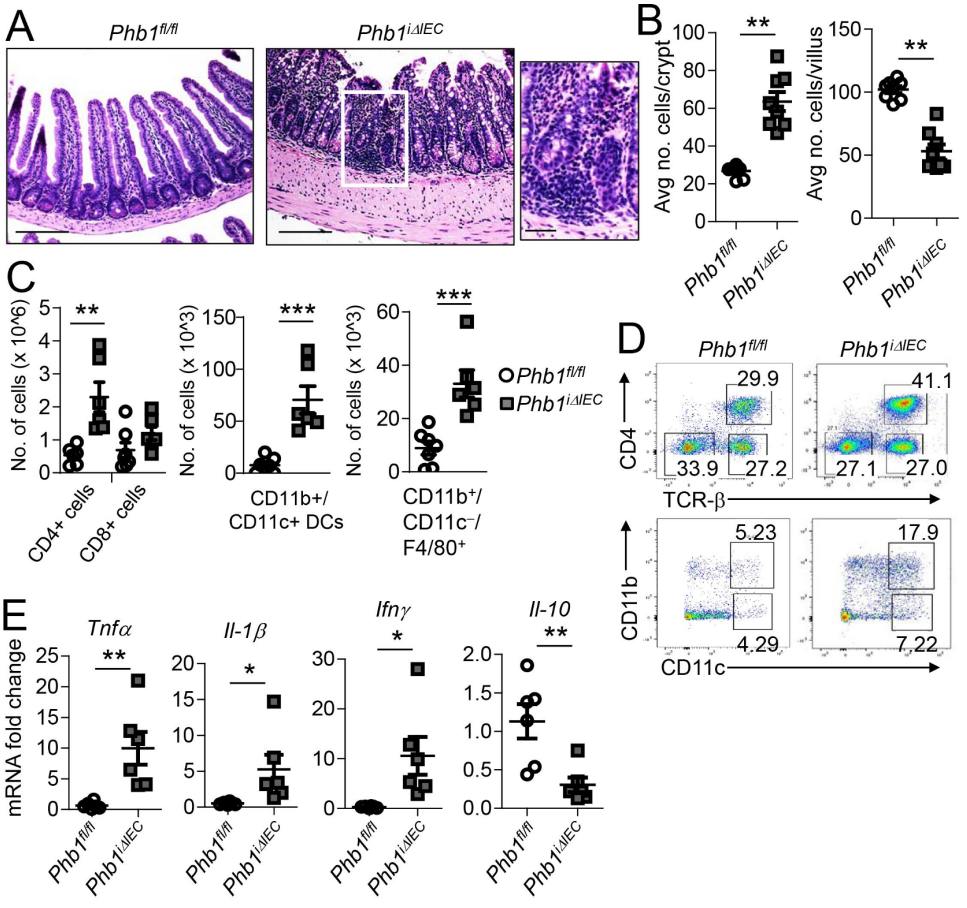

Figure 1 *Phb1*$^{i\Delta IEC}$ mice develop spontaneous ileitis 12 weeks after *Phb1* deletion. (A) H&E-stained sections showing ileum histology. Scale bars: 250 µm, boxed pullout: 75 µm. (B) The number of epithelial cells across 50 crypts or 50 villi per mouse. (C) Absolute number of ileal lamina propria (LP) immune cells calculated of total LP cells isolated from ileum. Data are representative of three independent experiments. (D) Representative flow cytometry plots gated on CD45$^+$ cells (top) or gated on CD45$^+$MHCII$^+$Gr-1$^-$B220$^-$Cells (bottom) (E) mRNA expression in ileum measured by qPCR. Results are presented as individual data points±SEM of 10 mice (B), 6-7 mice (1 *Phb1*^{i}*ΔIEC* outlier removed after Grubbs' test) (C), or 6 mice (E) per group. *P<0.05, **P<0.01, ***P<0.001 by unpaired, two-tailed Student's t-test. IFN-γ, interferon-γ; IL-10, interleukin-10; *Phb1*^{i}*ΔIEC*, intestinal epithelial cell deletion of *Phb1*; *Phb1*$^{\Delta PC}$, Paneth cell-specific deletion of *Phb1*; TNFα, tumour necrosis factor α.

thickening of the muscularis layers, crypt abscesses, crypt architectural changes including crypt branching, crypt elongation, and villus blunting (figure 1A,B, online supplementary figure S2C,D). *Phb1*$^{i\Delta IEC}$ mice exhibited splenomegaly and ileal infiltration of CD4$^+$ T cells, CD11b$^+$/CD11c$^+$ dendritic cells and F4/80$^+$ macrophages (figure 1C,D, online supplementary figure S2E). Expression of proinflammatory cytokines *Tnfα*, Interleukin-1*β* (*IL-1β*) and Interferon-γ (*Ifnγ*) was increased in *Phb1*$^{i\Delta IEC}$ ileum with a concomitant decrease in anti-inflammatory *Il-10* (figure 1E). Gut microbiota was altered in *Phb1*$^{i\Delta IEC}$ mice compared with *Phb1*$^{fl/fl}$ littermates, with decreased bacterial diversity and significant decreases in abundance of *Blautia*, *Roseburia*, *Coprococcus*, *Oscillibacter*, as has been reported as decreased in IBD patients,[15 16] as well as decreased abundance of *Marvinbryantia*, *Acetatifactor* and *Pseudoflavonifractor* (online supplementary figure S3). These bacterial alterations were observed 1 week after *Phb1* deletion and decreases in abundance of *Roseburia*, *Oscillibacter*, *Marvinbryantia* and *Acetatifactor* and Shannon Diversity were sustained through 12 weeks after *Phb1* deletion.

Ileal IECs exhibit mitochondrial dysfunction during deletion of *Phb1*

Since mitochondrial morphology is closely linked to function, mitochondria in epithelial cells of the ileum were visualised by transmission electron microscopy (TEM). Twelve weeks after induction of *Phb1* deletion, ileal epithelial cells demonstrated loss of microvilli and increased vacuolation (online supplementary figure S4). TUNEL$^+$ staining in ileal crypts and villi of *Phb1*$^{i\Delta IEC}$ mice suggest apoptosis and/or necrosis of the epithelium, confirmed by increased Cleaved caspase 3 expression (online supplementary figure S5A–C). A statistically significant proportion of the mitochondria of enterocytes, goblet cells, Paneth cells and crypt base columnar (CBC) stem cells of *Phb1*$^{i\Delta IEC}$ mice were unhealthy (swollen, dissolution/delocalisation of cristae) or contained electron-dense inclusion bodies as a reaction to injury[17] (figure 2A,B). Mitochondrial dysfunction in *Phb1*$^{i\Delta IEC}$ ileal IECs was also evident by decreased activity of ETC complexes I, II and IV (figure 2C) and the induction of the mitochondrial unfolded protein response (mtUPR; figure 2D), which is triggered on

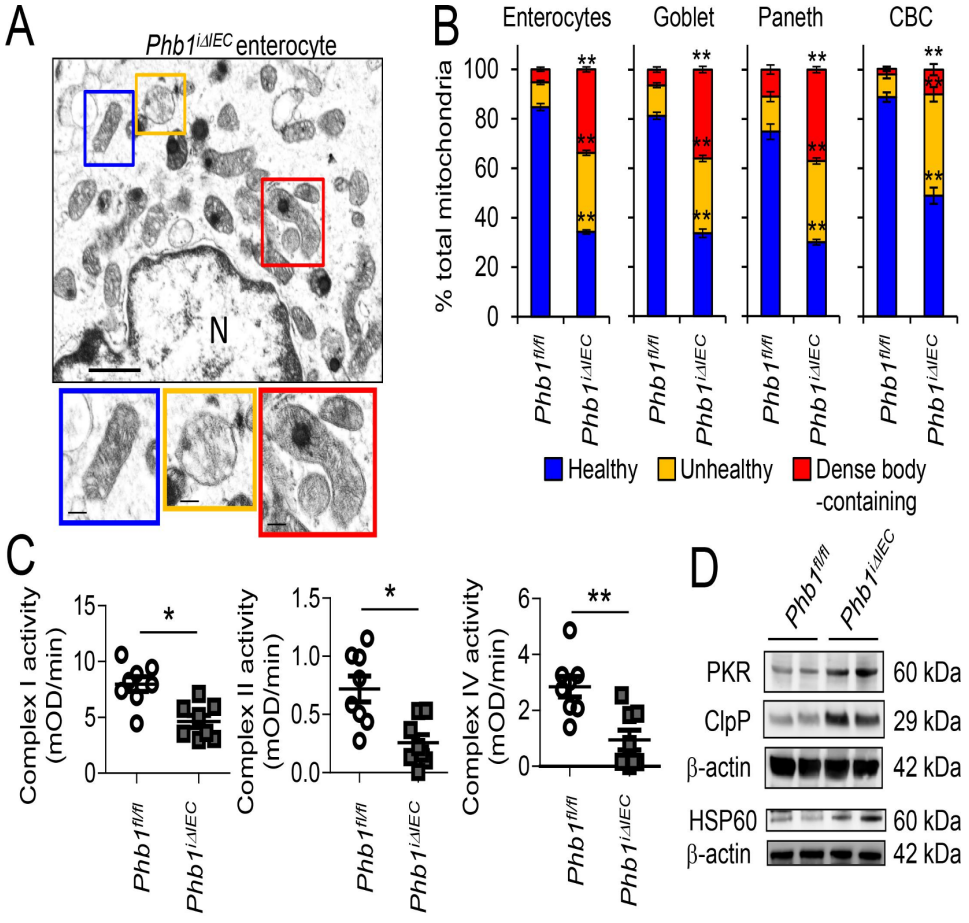

Figure 2 *Phb1*$^{i\Delta IEC}$ ileal IECs exhibit mitochondrial dysfunction. Time point shown is 12 weeks after *Phb1* deletion. (A) TEM of ileal enterocyte. Representative healthy (blue box), unhealthy (orange box), and dense inclusion body-containing (red box) mitochondria. Scale bars: 500 nm. N, nucleus. (B) % healthy, unhealthy, and dense inclusion body-containing mitochondria visualised by TEM. n=200 enterocytes, 200 goblet cells, 50 Paneth cells, and 50 CBC cells with an average of 42 mitochondrial/cell. Enteroendocrine cells were too sparse to quantitate. (C) ETC complex activity in isolated ileal IECs. (D) Representative Western blots of mtUPR markers in isolated ileal IECs. Results are presented as pooled data means±SEM (B) or as individual data points±SEM (C) of four mice per group (B) of eight mice per group (C, D). *P<0.05, **P<0.01 by 1-way ANOVA followed by Bonferroni's test (B) or by unpaired, 2-tailed Student's t-test (C). ANOVA, analysis of variance; CBC, crypt base columnar; ETC, electron transport chain; HSP, heat shock protein; IECs, intestinal epithelial cells; mtUPR, mitochondrial unfolded protein response; *Phb1*$^{i\Delta IEC}$, intestinal epithelial cell deletion of Phb1; PKR, protein kinase R; SEM, standard error mean; TEM, transmission electron microscopy.

Table 1 Proportion of *Phb1*$^{i\Delta IEC}$ mice that manifest mitochondrial dysfunction, abnormal Paneth and goblet cells, and histological inflammation

Week after *Phb1* deletion	Mice with mitochondrial dysfunction* N (%)	% mice with abnormal Paneth cells† n (%)	% mice with abnormal AB$^+$ cells‡n (%)	% mice with histological inflammation n (%)
1	12/12 (100)	4/12 (25)	0/12 (0)	0/12 (0)
3	12/12 (100)	7/12 (58)	2/12 (12)	2/12 (17)
6	N/D	10/14 (78)	6/14 (43)	6/14 (43)
12	15/15 (100)	13/15 (87)	13/15 (87)	13/15 (87)

*Defined as increased mtUPR, ultrastructural abnormalities in IECs by TEM.
†Defined as altered lysozyme staining, less abundant secretory granules, and AB$^+$ staining.
‡Defined as enlarged, more abundant AB$^+$ cells above the crypt base.
IEC, intestinal epithelial cell; mtPUR, mitochondrial unfolded protein response; N/D, not determined; Phb1$^{i\Delta IEC}$, intestinal epithelial cell deletion of Phb1; TEM, transmission electron microscopy.

accumulation of unfolded proteins within the mitochondrial matrix and is evident in epithelial cells from Crohn's disease and ulcerative colitis patients.[8] These mitochondrial changes did not significantly alter ATP concentration in isolated ileal IECs (online supplementary figure S6A), as has been shown previously in other cells with *Phb1* deficiency.[18 19]

Since mitochondrial dysfunction demonstrated in *Phb1*-deficient ileal IECs could be secondary to inflammation, we next determined whether earlier time points after the induction of *Phb1* deletion exhibited mitochondrial dysfunction. Mitochondrial ultrastructural abnormalities and mtUPR were induced in IECs as early as 1 week following *Phb1* deletion and was sustained through 12 weeks (online supplementary figure S6B–E). Upregulation of *Opa1*, which is a master regulator of mitochondrial fusion and bioenergetics, but not other genes controlling mitochondrial function (*Polg1*, *Polg2*, *Tfam* or *Pgc1*), was evident early after *Phb1* deletion in ileal IECs (online supplementary figure S6F). Additionally, endoplasmic reticulum (ER) stress and mitochondrial dysfunction can be interrelated during chronic inflammation with communication between the two organelles.[20] Indeed, upregulation of ER UPR markers coincides with mitochondrial dysfunction in *Phb1*$^{i\Delta IEC}$ ileal IECs (online supplementary figure S7A,B). Very few mice displayed histological inflammation of the ileum at early time points (1 or 3 weeks) following *Phb1* deletion (table 1), suggesting that mitochondrial dysfunction precedes ileitis in this model.

Mitochondria are the primary source of ROS with 0.2%–2.0% of oxygen consumed converted to superoxide by normal ETC activity. Mitochondrial dysfunction causes accumulation of mitochondrial-derived ROS (mtROS) due to blockade of forward electron flow through the ETC, subsequently causing more electrons to leak to oxygen. Oxidative damage to lipids and DNA is evident in the ileum of *Phb1*$^{i\Delta IEC}$ mice as early as 1 week after *Phb1* deletion (online supplementary figure S7C,D). Additionally, ROS-generating mitochondria have been shown to activate the $NLRP_3$ inflammasome, which in turn leads to caspase-1 dependent secretion of proinflammatory cytokines IL-1β and IL-18.[21] *Phb1*$^{i\Delta IEC}$ mice exhibit increased expression of active Caspase-1, IL-1β and IL-18 in ileum 1 week after *Phb1* deletion without altered expression of other proinflammatory cytokines or chemokines commonly upregulated in intestinal inflammation at this early time point (online supplementary figure S8).

Phb1$^{i\Delta IEC}$ mice exhibit ileal Paneth cell abnormalities early after *Phb1* deletion

During histological examination of H&E-stained ileum sections, alterations in Paneth cells, such as smaller secretory granules, were obvious in *Phb1*$^{i\Delta IEC}$ mice 12 weeks after *Phb1* deletion (figure 3A). Paneth cells contribute to gut homoeostasis by synthesising antimicrobial peptides and proteins such as lysozyme and defensins (also called cryptdins) and intestinal stem cell (ISC) niche factors.[22] IHC staining demonstrated that lysozyme$^+$ cells were expanded in number in *Phb1*$^{i\Delta IEC}$ mice (figure 3B,C). Lysozyme is normally efficiently packaged into secretory granules in Paneth cells as demonstrated in *Phb1*$^{fl/fl}$ mice (figure 3B). Ileal Paneth cells in *Phb1*$^{i\Delta IEC}$ mice exhibited altered patterns of lysozyme allocation (as previously described by[23 24]), with the majority showing diminished or diffuse lysozyme staining (figure 3B,D). Using these same criteria, 20%–50% of Crohn's disease patients have ≥20% abnormal Paneth cells (called Type I Paneth cell phenotype), which was associated with gut microbiota alterations and poor clinical outcomes such as early postoperative recurrence after resection.[25–27] Paneth cell granules in *Phb1*$^{i\Delta IEC}$ mice visualised by TEM were smaller and composed of an electron dense core and an enlarged electron-lucent peripheral halo compared with *Phb1*$^{fl/fl}$ mice (figure 3E). Previous studies have identified this electron-lucent halo in murine Paneth cells as predominantly containing Mucin2.[28] *Phb1*$^{i\Delta IEC}$ mice exhibited decreased mRNA expression of antimicrobials produced by Paneth cells such as *RegIIIγ*, *Cryptdin3*, *Cryptdin5* and *Ang4* (online supplementary figure S9A), suggesting loss of Paneth cell function vs simply degranulation of Paneth cell enzymes on a sustained basis.

Goblet-like cells containing dense core mucin granules, or a combination of mucin granules and abnormal Paneth cell granules, were observed in the crypt base of *Phb1*$^{i\Delta IEC}$ mice by TEM (figure 3E). Alcian blue (AB)–periodic acid schiff staining confirmed an increase in the number of AB$^+$ cells in the crypt base during *Phb1* deletion (figure 4A,B). Colocalisation of MUC2 (goblet cell marker) and lysozyme (Paneth cell marker) staining in the *Phb1*$^{i\Delta IEC}$ crypt base, evident in areas with and without inflammation, suggest these cells are 'intermediate' goblet/Paneth cells (figure 4C). These intermediate cells have been proposed to be Paneth cells undergoing transformation to goblet cells, goblet cells in the process of being converted to Paneth cells, or a precursor of both lineages. This altered differentiation programme in *Phb1*$^{i\Delta IEC}$ crypts was accompanied by increased TUNEL$^+$ staining and cell proliferation (online supplementary figure S5), suggesting increased turnover of the intestinal epithelium.

In addition to the appearance of intermediate cells in the ileal crypts of *Phb1*$^{i\Delta IEC}$ mice, AB$^+$ cells above the crypt base were increased in number and size with increased cytoplasmic mucin/cell (figure 4B–E). Examination of ileum at earlier time points after the induction of *Phb1* deletion demonstrated that crypt intermediate cells are evident before abnormal villus AB$^+$ cells (table 1 and online supplementary figure S9B,C). As early as 1 week after *Phb1* deletion, mRNA expression of goblet cell genes *Muc2* and *Muc4* are increased with a concomitant increase in *Klf4* and *Elf3* (online supplementary figure S9A), which are transcription factors involved in goblet cell differentiation. Phb1$^{i\Delta IEC}$ mice exhibited decreased mRNA expression of *Hes1* and increased *Math1* (online supplementary figure S9A), a situation that has been shown to promote secretory cell differentiation.[29] *Sox9*, which controls, at least in part, Paneth cell differentiation, and *Lgr5*, the intestinal CBC stem cell marker,

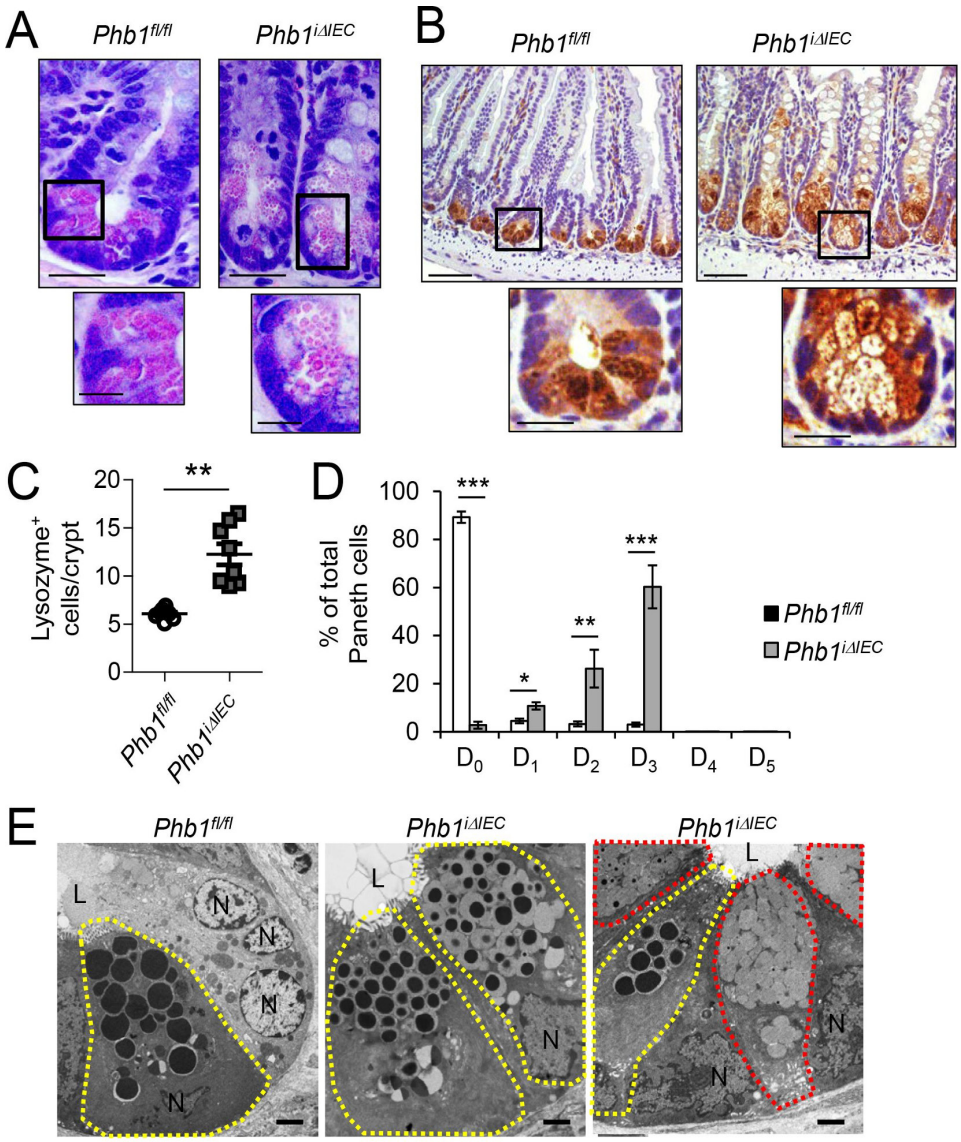

Figure 3 *Phb1*$^{\Delta IEC}$ mice exhibit ileal Paneth cell abnormalities. Time point shown is 12 weeks afetr *Phb1* deletion. (A) H&E-stained sections showing Paneth cells. Scale bars: 50 µm, boxed pullout: 20 µm. (B) Lysozyme IHC staining. Scale bars: 250 µm, boxed pullouts: 50 µm (C) The number of lysozyme+ cells across 50 crypts per mouse. (D) % of Paneth cells displaying each pattern of lysozyme expression. D0, normal; D1, disordered; D2, diminished; D3, diffuse; D4, excluded; D5, enlarged. 500 cells quantitated each mouse. (E) TEM of crypt base. Paneth cells, yellow outline; goblet-like cells, red outline. N, nucleus; L, lumen. Scale bars: 2 µm. Results are presented as individual data points±SEM (C) or as pooled data means± SEM (D) of 8 mice per group. **P<0.01, ***p<0.001 by unpaired, 2-tailed Student's t-test. (B) Or by 1-way ANOVA followed by Bonferroni's test (D). ANOVA, analysis of variance; *Phb1*$^{\Delta IEC}$, intestinal epithelial cell deletion of *Phb1*.

were not altered in *Phb1*$^{i\Delta IEC}$ mice (online supplementary figure S9A). FABP6 immunostaining suggests that enterocyte numbers are decreased by 12 weeks after *Phb1* deletion but not as early as 1 week, while enteroendocrine cells (marked by chromogranin A$^+$ expression) were unaffected in *Phb1*$^{i\Delta IEC}$ mice (online supplementary figure S10).

To determine the sequence of pathological events driving ileal inflammation in *Phb1*$^{i\Delta IEC}$ mice, the proportion of mice that manifest ileitis, Paneth cell or villus AB$^+$ cell abnormalities, or mitochondrial dysfunction at 1, 3, 6 or 12 weeks after the induction of *Phb1* deletion were quantitated. Mitochondrial dysfunction was evident in all mice at 1 week, Paneth cell abnormalities in the majority of mice beginning at 3 weeks, followed by villus AB$^+$ cell abnormalities and spontaneous ileitis, which developed in the majority of mice after 6 weeks (table 1). Collectively, these results demonstrate that the loss of *Phb1* causes mitochondrial dysfunction and subsequent Paneth cell defects prior to the onset of ileitis.

Mito-Tempo ameliorates mitochondrial dysfunction, Paneth cell defects and ileitis during loss of *Phb1*

To determine whether a mitochondrial-targeted antioxidant has therapeutic potential in Paneth cells, the dysfunction of which plays a role in the pathogenesis of Crohn's disease,[22] a subset of mice were treated daily for 3 weeks with Mito-Tempo concurrent with tamoxifen injections to induce *Phb1* deletion. Mito-Tempo is a mitochondrial-targeted superoxide dismutase 2 mimetic shown to have antioxidant properties.[30] Mito-Tempo ameliorated mitochondrial ultrastructural abnormalities and mtUPR and ER UPR responses in *Phb1*$^{i\Delta IEC}$ ileal IECs (figure 5A–C). Additionally, Mito-Tempo restored lysozyme staining and

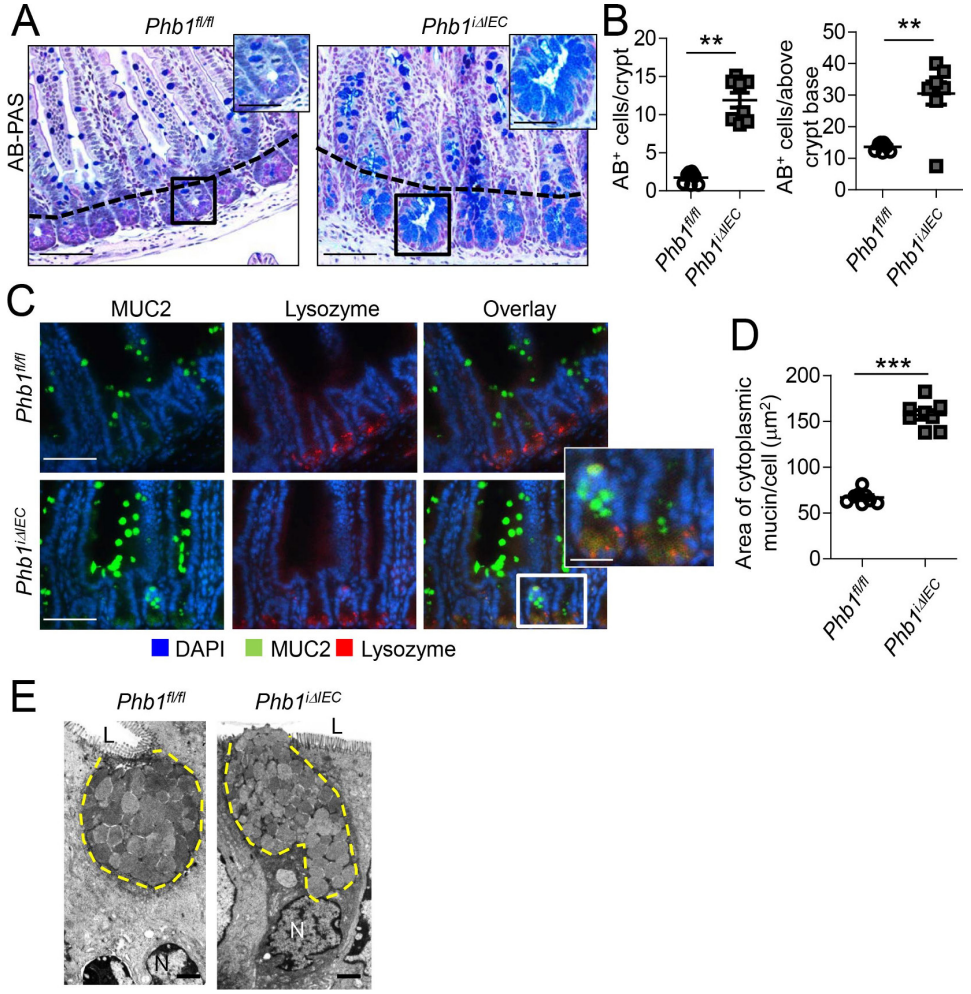

Figure 4 Ileal Paneth cells resemble goblet/Paneth intermediate cells and goblet cell number and size are increased in *Phb1*$^{i\Delta IEC}$ mice. Time point shown is 12 weeks after *Phb1* deletion (A) AB-PAS-stained sections. Dashed line denotes crypt base. Scale bars: 250 µm, boxed pullouts: 50 µm. (B) The number of AB^{+} cells in the crypt base (below dashed line in A) or above the crypt base across 50 crypts per mouse. (C) MUC2 (goblet cell marker) and Lysozyme (Paneth cell marker) immunofluorescene staining. Scale bars: 250 µm, boxed pullout showing co-localisation: 75 µm. (D) Quantitation of average mucin area/goblet cell above the crypt base. 250 cells quantitated each mouse. (E) TEM of villus goblet cells. Mucin granules, yellow outline. Scale bars: 1 µm. Results are presented as individual data points ± SEM of 8 mice per group. **P<0.01, ***p<0.001 by unpaired, 2-tailed student's t test. AB-PAS, alcian blue–periodic acid schiff; L, lumen; MUC2, mucin2; N, nucleus; *Phb1*$^{i\Delta IEC}$, intestinal epithelial cell deletion of *Phb1*; SEM, standard error mean; TEM, transmission electron microscopy.

Paneth cell antimicrobial expression such as *RegIIIγ*, *Cryptdin3* and *Cryptdin5* in Phb1$^{i\Delta IEC}$ mice (figure 5D,E). AB^{+} crypt cells and expression of *Muc2* and *Muc4* in *Phb1*$^{i\Delta IEC}$ mice treated with Mito-Tempo was similar to *Phb1*$^{fl/fl}$ mice (figure 5D,E), suggesting that Mito-Tempo prevented differentiation changes favouring intermediate cells during *Phb1* deletion. Mito-Tempo also prevented the upregulation of *Il-1β* and *Il-18* in the ileum that was induced during *Phb1* deletion (figure 5F). We continued administration of Mito-Tempo for an additional 9 weeks to assess severity of ileitis (figure 5G). Only 20% (2/10 mice) of *Phb1*$^{i\Delta IEC}$ mice treated with Mito-Tempo through 12 weeks exhibited histological evidence of inflammation in the ileum, compared with 80% (8/10 mice) of *Phb1*$^{i\Delta IEC}$ mice treated with vehicle.

Since Tempo not targeted to the mitochondria has been shown to affect microbiota,[31] we administered Mito-Tempo *in vitro* using ileal enteroids to eliminate microbiota as a confounding factor and to examine epithelial cell-intrinsic responses. Enteroids derived from *Phb1*$^{i\Delta IEC}$ mice formed fewer crypt buds and exhibited significant death during the 7-day culture period compared with enteroids derived from *Phb1*$^{fl/fl}$ mice (online supplementary figure S11A–C). *Phb1*$^{i\Delta IEC}$ enteroids also displayed activation of the mtUPR and ER UPR, increased production of mitochondrial-derived superoxide and loss of expression of Paneth cell antimicrobials *RegIIIγ*, *Cryptdin3*, *Cryptdin5* and *Ang4* (online supplementary figure S11F,G). Mito-Tempo decreased *Phb1*$^{i\Delta IEC}$ enteroid death, mitochondrial-derived superoxide production, mtUPR and ER UPR activation and restored expression of Paneth cell antimicrobials to that of *Phb1*$^{fl/fl}$ enteroids (online supplementary figure S11E–G). Mito-Tempo had no effect on crypt budding (online supplementary figure S11D). These results suggest that mtROS contributes to Paneth cell defects and loss of viability of the ISC niche during IEC *Phb1* deficiency.

Mice with Paneth cell-specific deletion of *Phb1* develop spontaneous ileitis

To delineate the role of mitochondrial dysfunction specifically in Paneth cells and its effect on ileitis, we generated two mouse lines with Paneth cell-specific deletion by crossing *Phb1*$^{fl/fl}$ mice to *Defa6-Cre* mice (*Phb1*$^{Defa6\Delta PC}$) and to *Mist1-CreER*^{T2} mice

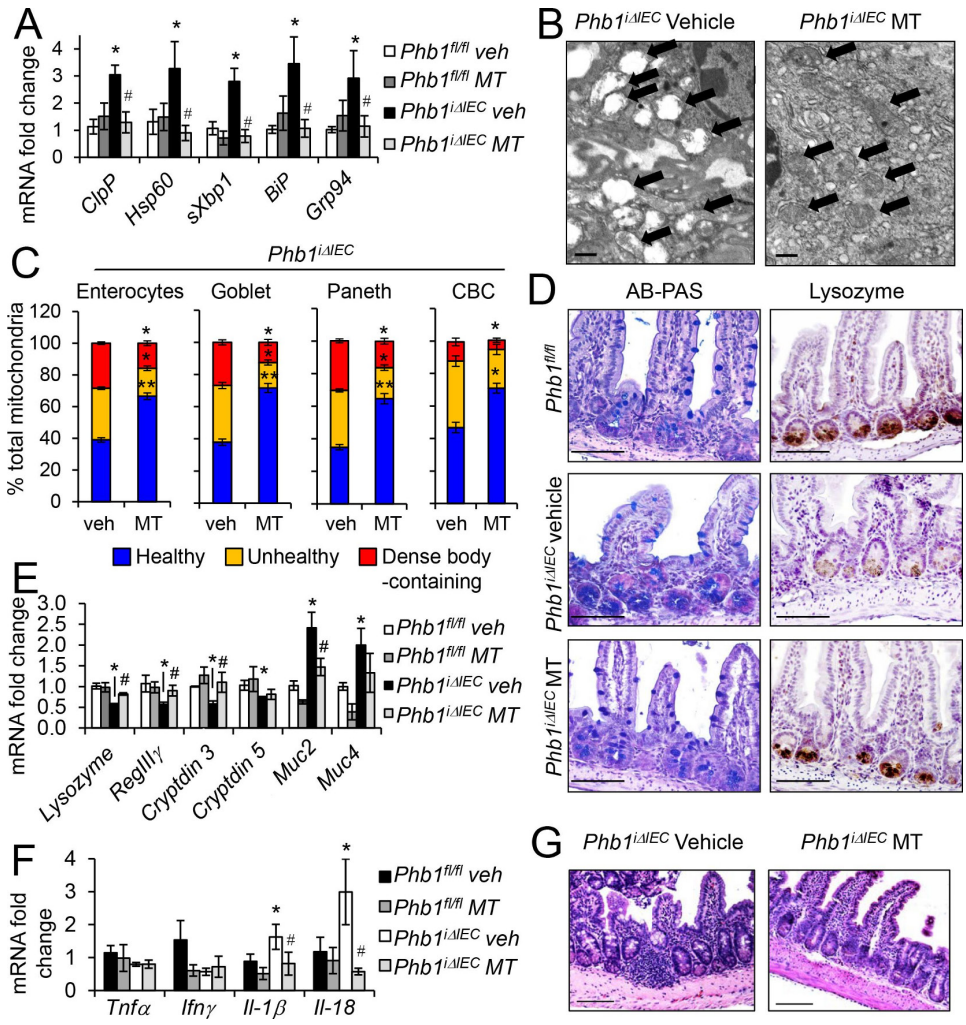

Figure 5 Mito-Tempo (MT) ameliorates mitochondrial dysfunction, Paneth cells defects, and ileitis in *Phb1*$^{i\Delta IEC}$ ileum. (A) mRNA expression of mtUPR (*ClpP, Hsp60*) and ER UPR (*sXbp1, BiP, Grp94*) markers in isolated ileal IECs measured by qPCR. (B) TEM of ileal enterocytes. Arrows indicate mitochondria. Scale bars: 500 nm. (C) % healthy, unhealthy (swollen, dissolution of cristae), and dense inclusion body-containing mitochondria visualized by TEM. n=200 enterocytes, 200 goblet cells, 50 Paneth cells, and 50 CBC cells with an average of 53 mitochondrial/cell. (D) AB-PAS and Lysozyme immunohistochemistry staining. Scale bars: 250 µm. mRNA expression in isolated ileal IECs (E) or whole ileum (F) measured by qPCR. (G) H&E-stained sections showing ileum histology at 12 weeks. Scale bars: 250 µm. Results are presented as pooled data means±SEM of 6 mice per group (A, E, F) or 4 mice per group (C). *P<0.05, **p<0.01 vs *Phb1*$^{fl/fl}$ veh, $^{\#}$p<0.05 vs *Phb1*$^{i\Delta IEC}$ veh by 1-way ANOVA followed by Bonferroni's test. AB-PAS, alcian blue–periodic acid schiff; ANOVA, analysis of variance; CBC, crypt base columnar; ER, endoplasmic reticulum; IECs, intestinal epithelial cells; IFN-γ, interferon-γ; IL-18, interleukin-18; mtUPR, mitochondrial unfolded protein response; *Phb1*$^{i\Delta IEC}$, intestinal epithelial cell deletion of *Phb1*; TEM, transmission electron microscopy; TNFα, tumour necrosis factor α.

(*Phb1*$^{iMist1\Delta PC}$). MIST1 (BHLHA15) is a critical transcription factor expressed in mature exocrine secretory cells like Paneth cells.[32] Robust expression of PHB1 was demonstrated in *Phb1*$^{fl/fl}$ mice and confirmed to be deficient in *Phb1*$^{Defa6\Delta PC}$ and *Phb1*$^{iMist1\Delta PC}$ mice (online supplementary figures S12A and S14A). *Phb1*$^{Defa6\Delta PC}$ and *Phb1*$^{iMist1\Delta PC}$ mice developed spontaneous, discontinuous ileitis with similar characteristics to that seen in *Phb1*$^{i\Delta IEC}$ mice such as infiltration of CD4^{+} T cells, CD11b^{+}/CD11c^{+} dendritic cells and F4/80^{+} macrophages, crypt elongation, villus blunting and thickening of the muscularis layers (figure 6A,B, online supplementary figures S12B, S14B–D). Inflammation was restricted to the ileum (online supplementary figures S12C and S14C). Despite these similarities, the penetrance of ileitis across *Phb1*$^{Defa6\Delta PC}$ and *Phb1*$^{iMist1\Delta PC}$ was lower than in *Phb1*$^{i\Delta IEC}$ mice (table 1 and online supplementary table S1). Much like *Phb1*$^{i\Delta IEC}$ mice, inflammation in *Phb1*$^{Defa6\Delta PC}$ and *Phb1*$^{iMist1\Delta PC}$ mice was associated with less body weight gain, enlarged spleens, and an early increase in *Il-1β* and *Il-18* expression followed by later increased *Tnfα* and *Ifnγ* and decreased *Il-10* (figure 6C, online supplementary figures S12D, S12E, S14E-F). Paneth cell abnormalities were evident as early as 1 week after the induction of *Phb1* deletion in *Phb1*$^{iMist1\Delta PC}$ mice and by 8 weeks of age in *Phb1*$^{Defa6\Delta PC}$, with altered lysozyme staining allocation pattern and increased AB^{+} staining (figure 6E–F, online supplementary figures S13A–C and S15A–F). Unlike *Phb1*$^{i\Delta IEC}$ mice, the number of lysozyme^{+} cells in *Phb1*$^{\Delta PC}$ crypts was decreased compared with *Phb1*$^{fl/fl}$ mice (figure 6D and online supplementary figure S15C). Goblet cells above the crypt base in *Phb1*$^{Defa6\Delta PC}$ and *Phb1*$^{iMist1\Delta PC}$ mice appeared similar to *Phb1*$^{fl/fl}$ mice throughout all time points studied (figure 6F, online supplementary figures S13D, S15F). Altered expression of Paneth cell antimicrobials, *Muc2* and *Muc4*, and *Hes1* and *Math1* in *Phb1*$^{Defa6\Delta PC}$ mice matched the expression pattern displayed by *Phb1*$^{i\Delta IEC}$ mice (online supplementary figure S13E).

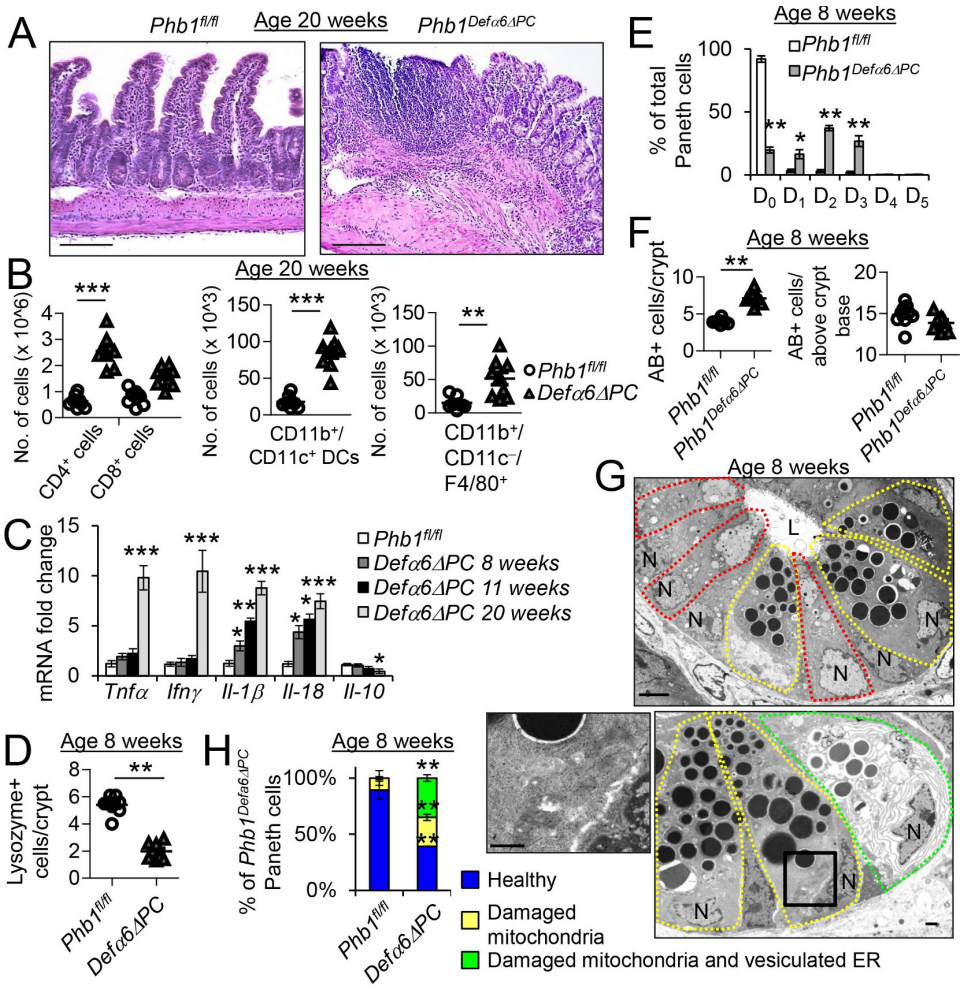

Figure 6 *Phb1*^{Defα6ΔC} mice develop mitochondrial dysfunction, Paneth cell defects, and spontaneous ileitis. (A) H&E-stained ileum sections at 20 weeks of age. Scale bars: 250 µm. (B) Absolute number of ileal LP immune cells calculated of total ileal LP cells. (C) mRNA expression in ileum measured by qPCR. (D) The number of Lysozyme$^+$ cells across 50 crypts per mouse. (E) % of Paneth cells displaying each pattern of Lysozyme expression. 50 cells quantitated each mouse. (F) The number of AB+ cells in the crypt base or above the crypt base across 50 crypts per mouse. (G) TEM of *Phb1*^{Defα6ΔPC} ileum crypt base. Paneth cells, yellow outline; goblet-like cells, red outline; Paneth cell with vesiculated ER, green outline. Scale bars: 1 µm. Box denotes area of higher magnification showing unhealthy mitochondria. (H) % of Paneth cells displaying vesiculated ER. Results are presented as individual data points ± SEM (B, D, F) or as pooled data means ± SEM (C, E) of 9 mice per group. *P<0.05, **p<0.01, ***p<0.001 vs PHB1$^{fl/fl}$ by unpaired, 2-tailed Student's t test (B, D, F) or by 1-way ANOVA followed by Bonferroni's test (C, E). ANOVA, analysis of variance; ER, endoplasmic reticulum; IL-10, interleukin-10; IFN-γ, interferon-γ; L, lumen; N, nucleus; TEM, transmission electron microscopy; TNFα, tumour necrosis factor α.

TEM analysis 1 week after *Phb1* deletion in *Phb1*^{Mist1ΔPC} mice and at 8 weeks of age in *Phb1*^{Defα6ΔPC} mice demonstrated similar mitochondrial ultrastructural changes in Paneth cells, but not other IECs, as those demonstrated in *Phb1*^{iΔIEC} mice (figure 6G, online supplementary figures S13F, S15G, and S15H). Enteroids derived from *Phb1*^{Defα6ΔPC} or *Phb1*^{iMist1ΔPC} mice exhibited decreased crypt budding similar to *Phb1*^{iΔIEC} enteroids, but less severe enteroid death and mitochondrial superoxide production compared with *Phb1*^{iΔIEC} enteroids that was further decreased by Mito-Tempo treatment (online supplementary figure S11B–F). Additionally, Paneth cells of *Phb1*^{Defα6ΔPC} and *Phb1*^{iMist1ΔPC} mice exhibited secretory granule alterations and the appearance of goblet/Paneth intermediate cells similar to *Phb1*^{iΔIEC} mice (figure 6G and online supplementary figure S15H). Interestingly, a significant proportion of *Phb1*^{Defα6ΔPC} and *Phb1*^{iMist1ΔPC} Paneth cells manifested vesiculated ER in addition to damaged mitochondria, suggesting severe ER stress which was corroborated by elevated ER UPR markers (figure 6G,H, online supplementary figures S13G, S15H, and S15I). A similar progression to ileitis was evident in *Phb1*^{Defα6ΔPC} and *Phb1*^{iMist1ΔPC} mice as was noted in *Phb1*^{iΔIEC} mice with initial mitochondrial dysfunction, followed by Paneth cell defects and subsequent ileal inflammation (table 1 and online supplementary table S1). Collectively, these results suggest that mitochondrial dysfunction due to *Phb1* deletion in Paneth cells is sufficient to drive ileitis.

DISCUSSION

Mitochondrial dysfunction is central to many chronic diseases, including arthritis, neurodegeneration, cardiovascular disease and cancer. Previous studies suggest a link between mitochondrial dysfunction and Crohn's disease. The paediatric RISK stratification study using RNA-sequencing analysis on Crohn's disease mucosal biopsies demonstrated that of patients who were at risk of stricturing, those who exhibited an enriched mitochondrial function gene signature remained complication free

through 36-month follow-up.[33] In a proteome study of paediatric Crohn's disease patients, impaired mitochondrial function was implicated and correlated with increased disease severity.[34] It was recently demonstrated that mtDNA is released into the serum in IBD patients and acts as a proinflammatory signalling molecule.[7] Deletion of *Irgm*, *Slc22A5*, *Pgc1α* or *Mdr1*, genes that serve roles in regulating mitochondrial health, cause spontaneous colitis or increase susceptibility to experimental colitis.[4 5] Well-characterised mouse models of spontaneous ileitis such as *SAMP1/Yit* or $TNF^{\Delta ARE}$ mice have not been examined for IEC mitochondrial dysfunction, but ileal histological alterations of $Phb1^{i\Delta IEC}$ or $Phb^{\Delta PC}$ mice were reminiscent to that of *SAMP1/Yit* mice.[35] Expression of PHB1 is decreased in mucosal biopsies from IBD-afflicted patients and in mouse models of colitis,[9 11] but the mechanism leading to decreased PHB1 expression in human IBD is unknown. IBD GWAS studies have not identified genetic mutation of *PHB1*. Genetic polymorphisms of *PHB1* have been associated with gastric, breast, ovarian and skin cancers with some studies implicating regulation at the 3′ UTR,[36] however, this has not been identified in IBD. Further studies are necessary to elucidate the mechanism of PHB1 deficiency during IBD.

Our results identify Paneth cells as highly susceptible to mitochondrial dysfunction driven by loss of *Phb1* and central to the pathogenesis of ileitis. A total of 70%–80% of Crohn's disease patients have inflammation involving the ileum, with or without colonic involvement. Mitochondrial dysfunction in IECs during *Phb1* deletion was evidenced by mitochondrial ultrastructural abnormalities, decreased activity of ETC complexes, increased mtROS and oxidative damage to lipids and DNA. These mitochondrial changes did not significantly alter ATP concentration in isolated ileal IECs, suggesting that IECs as a population have adequate energy production. Future studies will access individual IEC types like Paneth cells for ATP production. Mitochondrial health may be especially important in intestinal secretory cells (Paneth, goblet and enteroendocrine cells) which are mitochondria-rich to sustain energy-expending secretory functions. Additionally, mitochondrial dysfunction is likely to be especially deleterious in terminally differentiated long-lived cells, such as Paneth cells, in which damaged organelles are not diluted by cell replication.[22] Type I Paneth cell phenotype, characterised by ≥20% abnormal Paneth cells, defined by lysozyme granule staining characteristics (disordered, diminished, diffuse, enlarged or excluded) using mucosal biopsy samples,[27] occurs in approximately 20% of adult ileal Crohn's disease patients and is independent of active inflammation.[25 26] Crohn's disease-associated *ATG16L1 T300A* and *NOD2* risk alleles were shown to correlate with type I Paneth cell phenotype.[23 27] ATG16L1 and NOD2 play important roles in autophagy, an evolutionarily conserved catabolic pathway that removes cytoplasmic components, including damaged organelles, through lysosomal degradation. The autophagy pathway is crucial to suppress ileitis during *Xbp1* deletion in Paneth cells.[37] It is likely that mitophagy (autophagy of mitochondria) plays an important role in intestinal homoeostasis, but this has yet to be demonstrated in patients with IBD. Interestingly, patients with Crohn's disease with type I Paneth cell defects exhibited decreased expression of oxidative phosphorylation genes, suggesting this subset of patients may have altered mucosal mitochondrial function, but this was not further elucidated.[26] Our current results provide a mechanistic link between loss of PHB1, mitochondrial dysfunction and Paneth cell defects, which are three characteristics demonstrated in patients with Crohn's disease. Future studies will elucidate whether type I Paneth cell patients exhibit mitochondrial dysfunction, altered mitophagy or altered PHB1 expression.

mtROS are well-established primary downstream signalling molecules and, if excessive, mtROS can lead to cellular damage. Treatment of $Phb1^{i\Delta IEC}$ mice with the mitochondrial-targeted antioxidant Mito-Tempo ameliorated Paneth cell defects and ileitis during loss of *Phb1*. Mito-Tempo also prevented the upregulation of *Il-1β* and *Il-18* in the ileum of $Phb1^{i\Delta IEC}$ mice, suggesting that mtROS contributes to early increased secretion of these cytokines. Our results indicate that epithelial mitochondrial dysfunction evident 1 week after *Phb1* deletion concomitantly occurs with enhanced secretion of IL-1β and IL-18. Future studies will determine whether the mtROS signalling via the $NLRP_3$ inflammasome is involved in enhanced secretion of IL-1β and IL-18 in this model and the cellular source of these cytokines. Additionally, in *Phb1*-deficient enteroids, Mito-Tempo increased viability, decreased mtROS, decreased mtUPR and ER UPR activation, and restored expression of Paneth cell antimicrobials to that of $Phb1^{fl/fl}$ enteroids, suggesting epithelial cell-intrinsic responses to Mito-Tempo. These results demonstrate that mtROS contributes to Paneth cell defects and loss of viability of the ISC niche during IEC *Phb1* deficiency and present a druggable pathway for therapeutic targeting.

Mitochondrial function is a crucial modulator of stem cell fate in relatively quiescent stem cell populations, including haematopoietic stem cells and neural stem cells, as well as more active ISCs requiring more bioenergetics activity due to frequent turnover of the intestinal epithelium.[38] $Phb1^{i\Delta IEC}$ mice demonstrated Paneth/goblet intermediate cells early after *Phb1* deletion prior to signs of histological inflammation, followed by later increased number and size of goblet cells and decreased enterocytes. This altered differentiation programme in $Phb1^{i\Delta IEC}$ crypts was accompanied by increased crypt cell proliferation and apoptosis in crypts and villi, likely as a consequence of tissue repair induction. Goblet and Paneth cells differentiate from a common secretory cell lineage progenitor that is distinct from the enterocyte cell lineage progenitor.[29] Differentiation towards the secretory cell lineage is mediated by at least two transcription factors, Hes1 and Math1, which are altered in $Phb1^{i\Delta IEC}$ mice in a manner shown to favour secretory cell differentiation. Additionally, *Klf4* is increased in $Phb1^{i\Delta IEC}$ ileum and has been shown to be required for goblet cell-differentiation.[39] Intermediate cells in $Phb1^{i\Delta IEC}$ mice could originate from changes in the Paneth cell itself to promote transformation to a goblet cell, goblet cells being converted to Paneth cells, or stem cell responses driving altered lineage differentiation. It was previously shown that ISC mitochondrial dysfunction and decreased ability to produce ATP results in altered ISC self-renewal and proliferation.[38] We speculate that altered Paneth/goblet cell differentiation in ileum of $Phb1^{i\Delta IEC}$ mice could be due to (1) PHB1 directly regulating the Notch-1 (upstream of Hes1/Math1) and/or Klf4 pathways, (2) modulation of Notch-1 and/or Klf4 by redox-dependent signalling or mitochondrial dysfunction subsequent to PHB1 deletion and/or (3) a response to inflammation, however, this seems unlikely since altered secretory allocation was demonstrated preceding histological signs of inflammation. Additionally, IL-18 plays an important role in goblet cell differentiation[40 41] and future studies will assess whether the Paneth/goblet intermediate cells observed in $Phb1^{i\Delta IEC}$ mice are driven by IL-18 to prevent goblet cell maturation.

Paneth cell-specific deletion of *Phb1* induced a similar progression to ileitis as was demonstrated in $Phb1^{i\Delta IEC}$ mice with initial mitochondrial dysfunction and Paneth cell defects. At early time points, mitochondrial dysfunction was evident in only Paneth cells in $Phb1^{\Delta PC}$ mice, and not other IECs, confirming the importance of a healthy mitochondrial pool in Paneth cells

in maintaining intestinal homoeostasis. Penetrance of inflammation across *Phb1*$^{\Delta PC}$ mice was less than *Phb1*$^{i\Delta IEC}$ mice, suggesting mitochondrial dysfunction throughout the intestinal epithelium, as in *Phb1*$^{i\Delta IEC}$ mice, accelerates the progression to inflammation. Indeed, enteroids derived from *Phb1*$^{i\Delta IEC}$ mice exhibited more severe death and mitochondrial superoxide production compared with *Phb1*$^{Defa6\Delta PC}$ or *Phb1*$^{iMist1\Delta PC}$ enteroids. Unlike in *Phb1*$^{i\Delta IEC}$ mice, AB^{+} cells above the crypt base in *Phb1*$^{Defa6\Delta PC}$ and *Phb1*$^{iMist1\Delta PC}$ mice appeared normal throughout all time points examined with no alteration of *Klf4* or *Elf3* expression. This suggests *Phb1* deletion in ISCs or in goblet cells themselves drives goblet cell abnormalities in *Phb1*$^{i\Delta IEC}$ mice that is not recapitulated during Paneth cell-specific *Phb1* deletion. Similar to *Phb1*$^{i\Delta IEC}$ mice, *Phb1*$^{iMist1\Delta PC}$ mice developed Paneth cell defects and the appearance of intermediate cells at a time point (1 week) prior to normal turnover of Paneth cells (every 30–60 days[22]). This suggests that mitochondrial dysfunction in Paneth cells could trigger Paneth cell-intrinsic dedifferentiation to intermediate cells. Alternatively, death of Paneth cells could be accelerated in the *Phb1* deficient mice and as a repair response, an ISC-derived effect could give rise to intermediate cells. Given the close proximity of Paneth cells and ISCs and the known interrelationship of Paneth cell mitochondrial metabolism and ISC niche homoeostasis,[42] loss of *Phb1* in Paneth cells could in turn signal to alter ISC differentiation response. Future studies using reporter mice will elucidate whether Paneth cells or ISCs trigger altered IEC differentiation during loss of *Phb1*.

In summary, our findings further our understanding of intestinal homoeostasis originating at the cellular (Paneth cell) level and organellar (mitochondria) level. We identify Paneth cells as highly susceptible to mitochondrial dysfunction driven by *Phb1* deletion and central to the development of ileitis. Treatment of Paneth cell defects with Mito-Tempo during *Phb1* deletion implicates a potential therapeutic application for abnormal Paneth cells via elimination of mtROS. Mitochondrial-targeted therapeutics may have translational utility in a subset of patients with Crohn's disease exhibiting Paneth cell defects. These are the first results presenting a causative role of mitochondrial dysfunction in ileitis that initiates in Paneth cells.

MATERIALS AND METHODS

Materials and methods are included in the online supplementary materials.

Author affiliations
[1]Department of Medicine, Baylor Scott and White Research Institute, Dallas, Texas, USA
[2]Veterans Affairs North Texas Health Care System, Dallas, Texas, USA
[3]University of Texas Southwestern Medical Center at Dallas, Dallas, Texas, USA
[4]Gastroenterology and Hepatology, Veteran Affairs North Texas Health Care System, Dallas, Texas, USA
[5]Department of Medicine, Baylor Scott and White Center for Esophageal Research, Dallas, Texas, USA
[6]Internal Medicine, Washington University in Saint Louis School of Medicine, Saint Louis, Missouri, USA
[7]Brigham and Womens Hospital, Boston, Massachusetts, USA
[8]Morehouse School of Medicine, Atlanta, Georgia, USA

Acknowledgements We thank Jie Han and Arwa S Kathiria for technical assistance and Beth Cook for histology processing (Baylor Scott & White Research Institute). We are grateful to P Kay Lund and Amanda Mah (University of North Carolina at Chapel Hill, NC) for assistance with enteroid culturing. We thank Ricardo Olivarez and Stephanie Kara at the Anatomic Pathology Laboratory at Children's Health Medical Centre Dallas, Texas, USA, for assistance with electron microscopy.

Contributors Study concept and design: TD, LAF, RFS, RSB, KV and ALT. Acquisition of data: DNJ, MP, WLN, KT, LT-S and ALT. Analysis and interpretation of data: MP, WLN, KT, BLC, LT-S, KV and ALT. Drafting the manuscript: DNJ, MP and ALT. Critical revision of the manuscript for important intellectual content: TD, LAF, RFS, JCM, RSB, KV and WET.

Funding This work was supported by National Institutes of Health grants R01-DK117001 (ALT), R01-DK105129 (JCM), R01-DK088199 (RSB), R03-DK098229 (ALT) and Litwin IBD Pioneers Crohn's Colitis Foundation 301869 (ALT).

Competing interests None declared.

Patient and public involvement Patients and/or the public were not involved in the design, or conduct, or reporting, or dissemination plans of this research.

Patient consent for publication Not required.

Ethics approval Baylor Scott & White Research Institute Institutional Animal Care and Use Committee.

Provenance and peer review Not commissioned; externally peer reviewed.

Data availability statement All data relevant to the study are included in the article or uploaded as online supplementary information. All mice described in this study must be obtained through an MTA.

ORCID iDs
Themistocles Dassopoulos http://orcid.org/0000-0003-2968-0321
Rhonda F Souza http://orcid.org/0000-0003-3484-2807
Arianne L Theiss http://orcid.org/0000-0003-2862-0933

REFERENCES

1 Ray K. IBD: the changing epidemiology of IBD. *Nat Rev Gastroenterol Hepatol* 2017;14:690.
2 Kim DH, Cheon JH. Pathogenesis of inflammatory bowel disease and recent advances in biologic therapies. *Immune Netw* 2017;17:25–40.
3 Liu JZ, van Sommeren S, Huang H, *et al*. Association analyses identify 38 susceptibility loci for inflammatory bowel disease and highlight shared genetic risk across populations. *Nat Genet* 2015;47:979–86.
4 Ho G-T, Aird RE, Liu B, *et al*. MDR1 deficiency impairs mitochondrial homeostasis and promotes intestinal inflammation. *Mucosal Immunol* 2018;11:120–30.
5 Jackson DN, Theiss AL. Gut bacteria signaling to mitochondria in intestinal inflammation and cancer. *Gut Microbes* 2019:1–20.
6 Rath E, Moschetta A, Haller D. Mitochondrial function - gatekeeper of intestinal epithelial cell homeostasis. *Nat Rev Gastroenterol Hepatol* 2018;15:497–516.
7 Boyapati RK, Dorward DA, Tamborska A, *et al*. Mitochondrial DNA is a pro-inflammatory damage-associated molecular pattern released during active IBD. *Inflamm Bowel Dis* 2018;24:2113–22.
8 Rath E, Berger E, Messlik A, *et al*. Induction of dsRNA-activated protein kinase links mitochondrial unfolded protein response to the pathogenesis of intestinal inflammation. *Gut* 2012;61:1269–78.
9 Theiss AL, Idell RD, Srinivasan S, *et al*. Prohibitin protects against oxidative stress in intestinal epithelial cells. *Faseb J* 2007;21:197–206.
10 Nijtmans LG, de Jong L, Artal Sanz M, *et al*. Prohibitins act as a membrane-bound chaperone for the stabilization of mitochondrial proteins. *Embo J* 2000;19:2444–51.
11 Hsieh S-Y, Shih T-C, Yeh C-Y, *et al*. Comparative proteomic studies on the pathogenesis of human ulcerative colitis. *Proteomics* 2006;6:5322–31.
12 Theiss AL, Laroui H, Obertone TS, *et al*. Nanoparticle-based therapeutic delivery of prohibitin to the colonic epithelial cells ameliorates acute murine colitis. *Inflamm Bowel Dis* 2011;17:1163–76.
13 Theiss AL, Vijay-Kumar M, Obertone TS, *et al*. Prohibitin is a novel regulator of antioxidant response that attenuates colonic inflammation in mice. *Gastroenterology* 2009;137:199–208.
14 McClung JK, Jupe ER, Liu XT, *et al*. Prohibitin: potential role in senescence, development, and tumor suppression. *Exp Gerontol* 1995;30:99–124.
15 Hedin CR, McCarthy NE, Louis P, *et al*. Altered intestinal microbiota and blood T cell phenotype are shared by patients with Crohn's disease and their unaffected siblings. *Gut* 2014;63:1578–86.
16 Mondot S, Kang S, Furet JP, *et al*. Highlighting new phylogenetic specificities of Crohn's disease microbiota. *Inflamm Bowel Dis* 2011;17:185–92.
17 Colbourne F, Sutherland GR, Auer RN. Electron microscopic evidence against apoptosis as the mechanism of neuronal death in global ischemia. *J Neurosci* 1999;19:4200–10.
18 Artal-Sanz M, Tavernarakis N. Prohibitin couples diapause signalling to mitochondrial metabolism during ageing in C. elegans. *Nature* 2009;461:793–7.
19 Liu D, Lin Y, Kang T, *et al*. Mitochondrial dysfunction and adipogenic reduction by prohibitin silencing in 3T3-L1 cells. *PLoS One* 2012;7:e34315.

20 Rath E, Haller D. Mitochondria at the interface between danger signaling and metabolism: role of unfolded protein responses in chronic inflammation. *Inflamm Bowel Dis* 2012;18:1364–77.
21 Liu Q, Zhang D, Hu D, *et al*. The role of mitochondria in NLRP3 inflammasome activation. *Mol Immunol* 2018;103:115–24.
22 Clevers HC, Bevins CL. Paneth cells: maestros of the small intestinal crypts. *Annu Rev Physiol* 2013;75:289–311.
23 Cadwell K, Liu JY, Brown SL, *et al*. A key role for autophagy and the autophagy gene Atg16l1 in mouse and human intestinal Paneth cells. *Nature* 2008;456:259–63.
24 Cadwell K, Patel KK, Maloney NS, *et al*. Virus-plus-susceptibility gene interaction determines Crohn's disease gene Atg16L1 phenotypes in intestine. *Cell* 2010;141:1135–45.
25 Liu T-C, Gao F, McGovern DPB, *et al*. Spatial and temporal stability of paneth cell phenotypes in Crohn's disease: implications for prognostic cellular biomarker development. *Inflamm Bowel Dis* 2014;20:646–51.
26 Liu T-C, Gurram B, Baldridge MT, *et al*. Paneth cell defects in Crohn's disease patients promote dysbiosis. *JCI Insight* 2016;1:e86907.
27 VanDussen KL, Liu T-C, Li D, *et al*. Genetic variants synthesize to produce paneth cell phenotypes that define subtypes of Crohn's disease. *Gastroenterology* 2014;146:200–9.
28 Stahl M, Tremblay S, Montero M, *et al*. The MUC2 mucin coats murine Paneth cell granules and facilitates their content release and dispersion. *Am J Physiol Gastrointest Liver Physiol* 2018;315:G195–205.
29 Yang Q, Bermingham NA, Finegold MJ, *et al*. Requirement of Math1 for secretory cell lineage commitment in the mouse intestine. *Science* 2001;294:2155–8.
30 Dikalova AE, Bikineyeva AT, Budzyn K, *et al*. Therapeutic targeting of mitochondrial superoxide in hypertension. *Circ Res* 2010;107:106–16.
31 Aytekin FO, Teke Z, Aydin C, *et al*. Effects of a membrane-permeable radical scavenger, tempol, on healing of colonic anastomoses in the cecal ligation and puncture model of polymicrobial sepsis in rats. *Am J Surg* 2007;193:723–9.
32 Lo H-YG, Jin RU, Sibbel G, *et al*. A single transcription factor is sufficient to induce and maintain secretory cell architecture. *Genes Dev* 2017;31:154–71.
33 Kugathasan S, Denson LA, Walters TD, *et al*. Prediction of complicated disease course for children newly diagnosed with Crohn's disease: a multicentre inception cohort study. *Lancet* 2017;389:1710–8.
34 Mottawea W, Chiang C-K, Mühlbauer M, *et al*. Altered intestinal microbiota-host mitochondria crosstalk in new onset Crohn's disease. *Nat Commun* 2016;7:13419.
35 Vidrich A, Buzan JM, Barnes S, *et al*. Altered epithelial cell lineage allocation and global expansion of the crypt epithelial stem cell population are associated with ileitis in SAMP1/YitFc mice. *Am J Pathol* 2005;166:1055–67.
36 Chowdhury D, Kumar D, Sarma P, *et al*. PHB in cardiovascular and other diseases: present knowledge and implications. *Curr Drug Targets* 2017;18:1836–51.
37 Adolph TE, Tomczak MF, Niederreiter L, *et al*. Paneth cells as a site of origin for intestinal inflammation. *Nature* 2013;503:272–6.
38 Berger E, Rath E, Yuan D, *et al*. Mitochondrial function controls intestinal epithelial stemness and proliferation. *Nat Commun* 2016;7:13171.
39 Katz JP, Perreault N, Goldstein BG, *et al*. The zinc-finger transcription factor KLF4 is required for terminal differentiation of goblet cells in the colon. *Development* 2002;129:2619–28.
40 Nowarski R, Jackson R, Gagliani N, *et al*. Epithelial IL-18 equilibrium controls barrier function in colitis. *Cell* 2015;163:1444–56.
41 Pu Z, Che Y, Zhang W, *et al*. Dual roles of IL-18 in colitis through regulation of the function and quantity of goblet cells. *Int J Mol Med* 2019;43:2291–302.
42 Rodríguez-Colman MJ, Schewe M, Meerlo M, *et al*. Interplay between metabolic identities in the intestinal crypt supports stem cell function. *Nature* 2017;543:424–7.

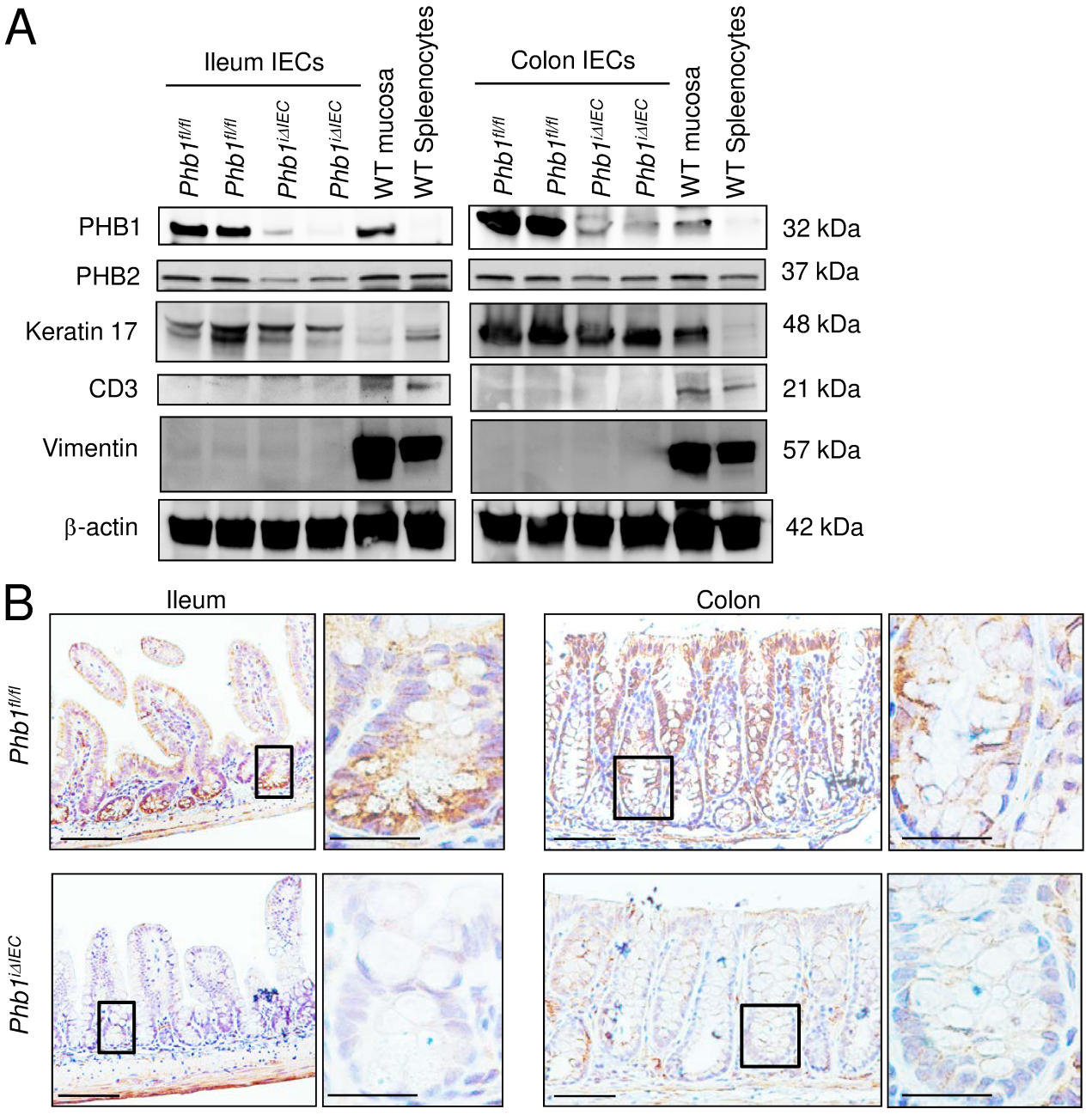

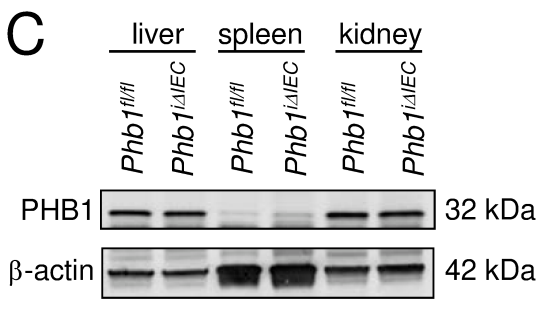

Fig. S1. Characterizing loss of PHB1 in *Phb1*$^{i\Delta IEC}$ mice. (**A**) Representative western blots of PHB1 expression in isolated ileal or colon epithelial cells. Blots were stripped and re-probed for Keratin 17 (a marker of epithelial cells), CD3 (a marker of immune cells), and Vimentin (a marker of fibroblasts) to ensure purity of epithelial isolation. (**B**) PHB1 immunohistochemistry staining. Scale bars: 250 μm, boxed pullout: 75 μm. (**C**) PHB1 protein expression in liver, spleen, and kidney is not altered in *Phb1*$^{i\Delta IEC}$ mice.

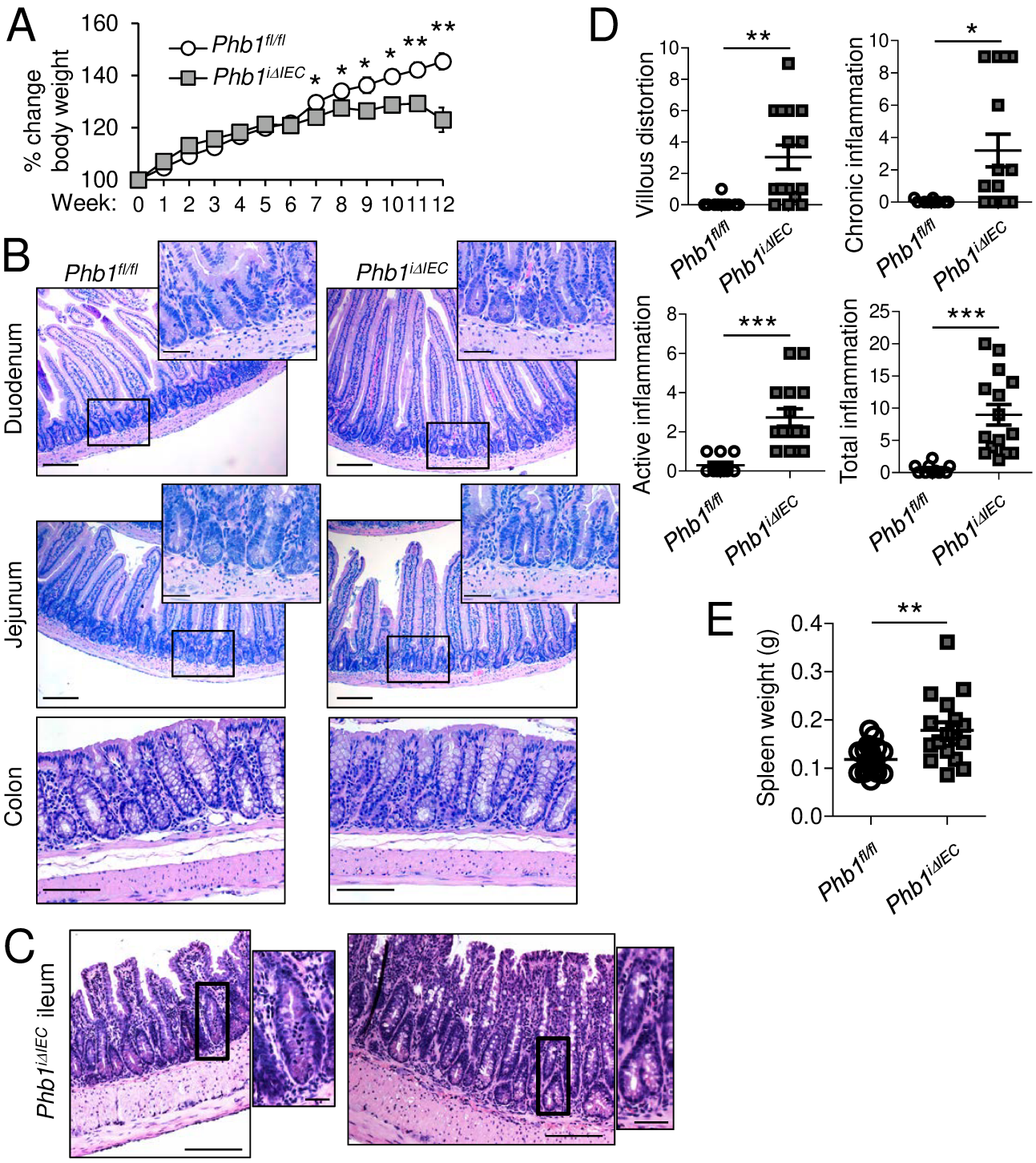

Fig. S2. Characterization of *Phb1*$^{i\Delta IEC}$ mice 12 weeks after *Phb1* deletion. (**A**) % body weight change. (**B**) Histology of duodenum, jejunum, and colon. (**C**) Examples of histology of ileum from *Phb1*$^{i\Delta IEC}$ mice. Left pullout shows a crypt abscess. Right pullout shows crypt branching. (**D**) Histological scoring of ileum by a blinded GI pathologist. (**E**) Spleen weight. Results are presented as pooled data means ± SEM (**A**) or individual data points ± SEM (**D**, **E**) of 18 *Phb1*$^{fl/fl}$ and 17 *Phb1*$^{i\Delta IEC}$ mice (**A**, **E**) or 10 *Phb1*$^{fl/fl}$ and 15 *Phb1*$^{i\Delta IEC}$ mice (**D**) per group. **P* < 0.05 ***P* < 0.01 ****P* < 0.001 by unpaired, 2-tailed Student's t test (**D**, **E**) or by 1-way ANOVA followed by Bonferroni's test (**A**). Scale bars: 250 μm, boxed pullouts: 75 μm.

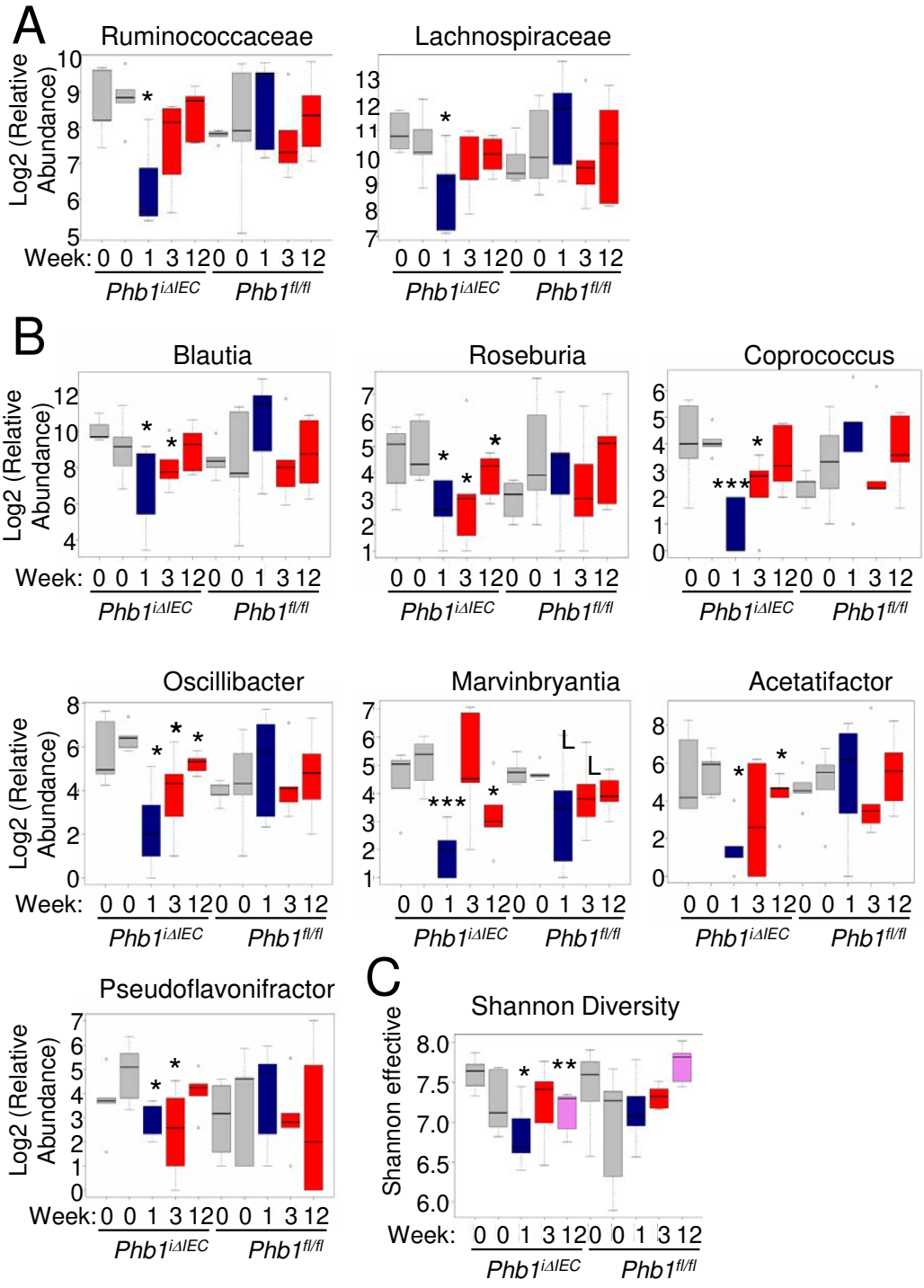

Fig. S3. Gut microbiota is altered in *Phb1*$^{i\Delta IEC}$ mice. Stool was collected from *Phb1*$^{fl/fl}$ and *Phb1*$^{i\Delta IEC}$ mice at baseline prior to tamoxifen injection to induce deletion of *Phb1* (week 0, two separate collections 1 day apart) and 1, 3, and 12 weeks after *Phb1* deletion. 16S ribosomal RNA gene amplicon in feces were sequenced on a MiSeq platform. (**A**) Changes in stool bacterial composition at the family level. (**B**) Changes in stool bacterial composition at the genus level. (**C**) Intestinal bacterial diversity. Taxonomic differences reported by Metastats with 95% CI of 5 mice per group. **P* < 0.05, ***P* < 0.01, ***P < 0.005.

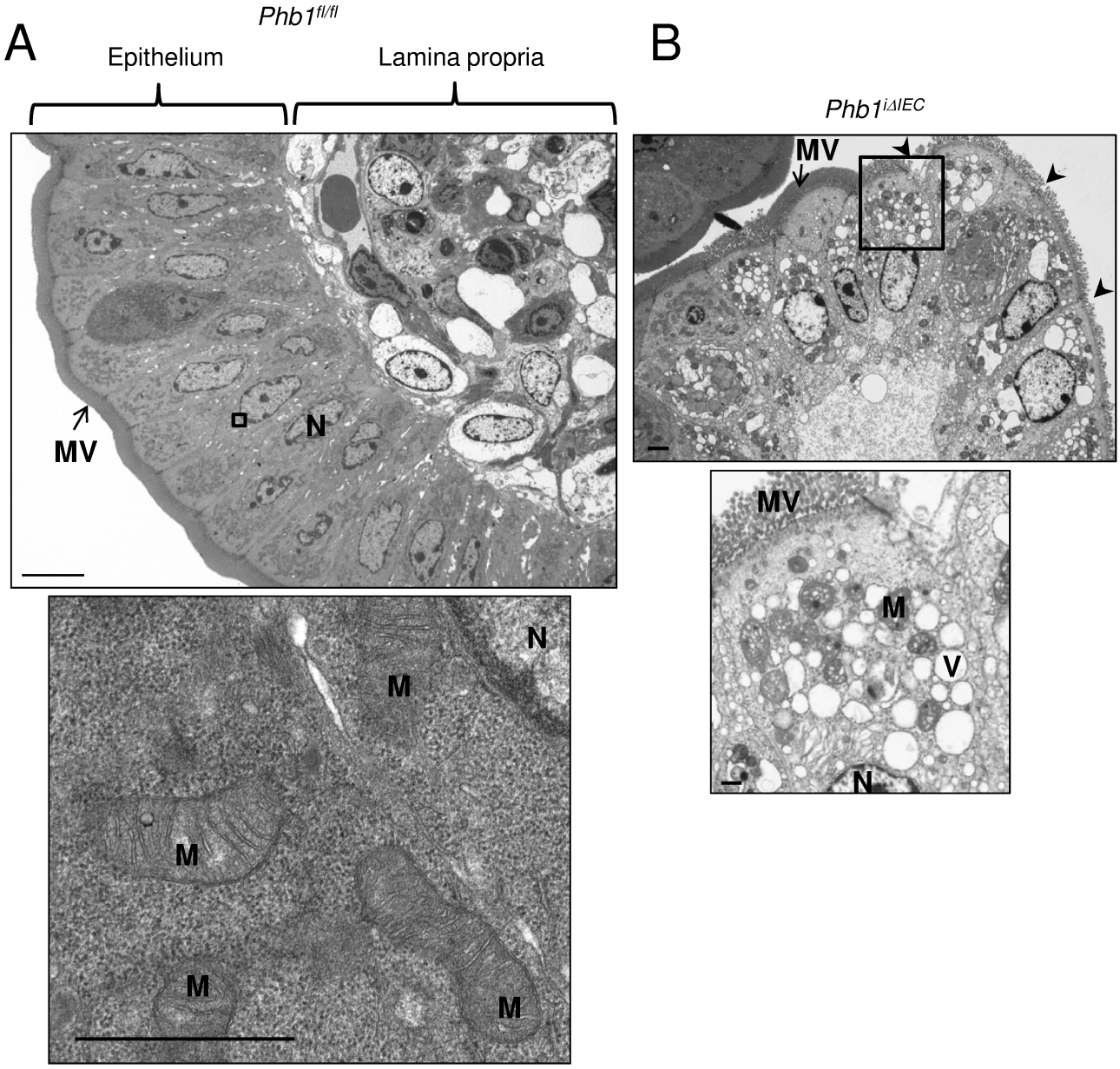

Fig. S4. Characterization of ileum epithelium by TEM during *Phb1* deletion. (**A**) *Phb1*$^{fl/fl}$ epithelium demonstrate healthy microvilli (MV). Boxed pullout shows healthy mitochondria (M). Scale bar: 10 μm, pullout below: 500 nm. (**B**) *Phb1*$^{i\Delta IEC}$ epithelial cells show dengeneration of the apical surface epithelium including loss of or disrupted microvilli (arrowheads) and increased vacuolation (V). Mitochondria are swollen, degenerative, and possess one or more electron-dense inclusion bodies. Scale bar: 4 μm, pullout below: 500 nm. N, nucleus.

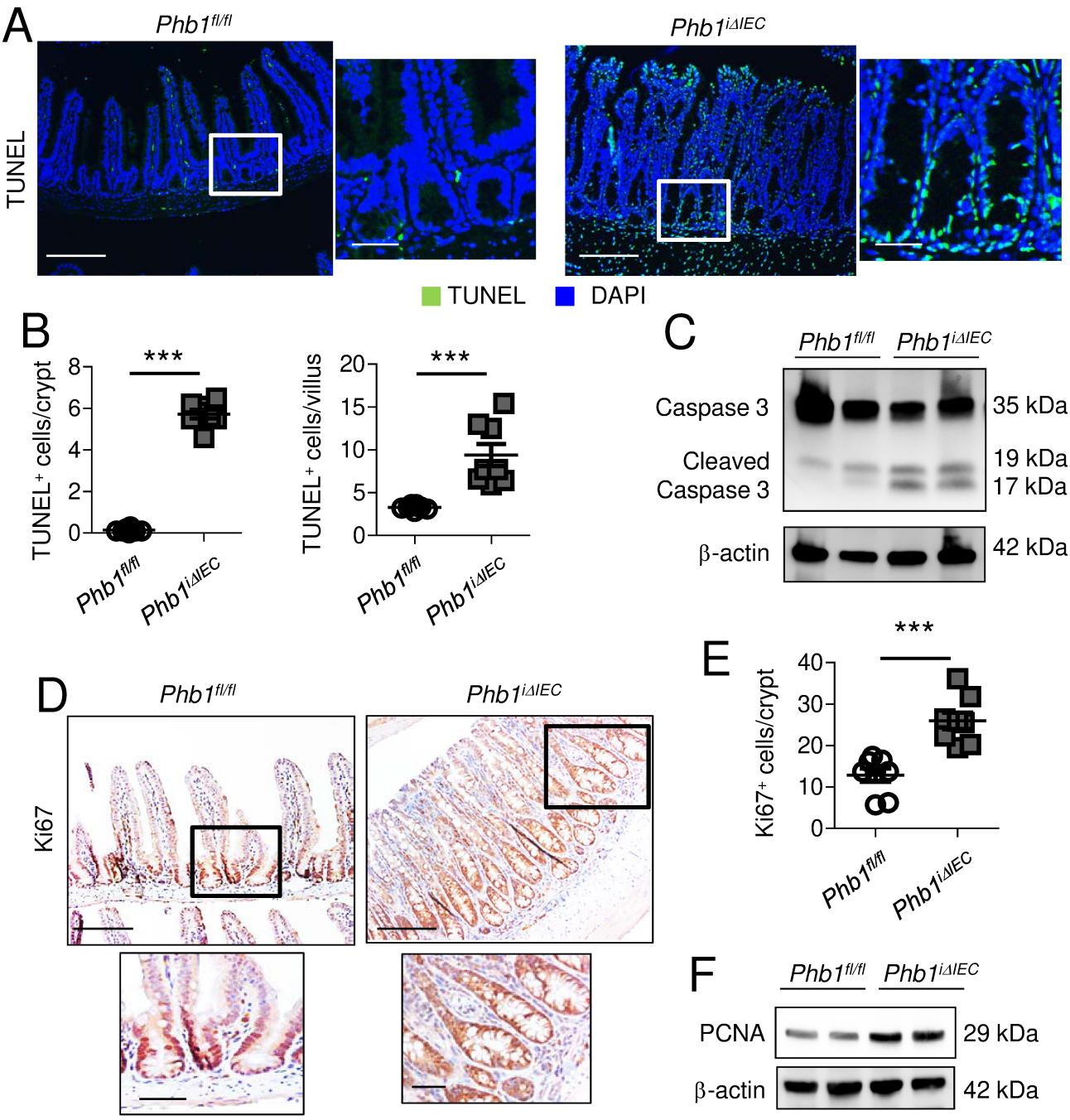

Fig. S5. *Phb1*$^{i\Delta IEC}$ mice exhibit increased ileal epithelial cell apoptosis and proliferation. (**A**) Photomicrographs of TUNEL (green) and DAPI (blue) staining. Scale bars: 250 μm, boxed pullouts: 75 μm. (**B**) The number of TUNEL$^+$ cells across 50 crypts or 50 villi per mouse. (**C**) Representative western blots of Cleaved Caspase 3 (marker of apoptosis) in isolated ileal IECs. (**D**) Ki67 IHC staining. Scale bars: 250 μm, boxed pullouts: 75 μm. (**E**) The number of Ki67$^+$ cells across 50 crypts per mouse. (**F**) Representative western blots of PCNA (marker of proliferation) in isolated ileal IECs. Results are presented as individual data points ± SEM of 8 mice per group. ***$P < 0.001$ by unpaired, 2-tailed Student's t test.

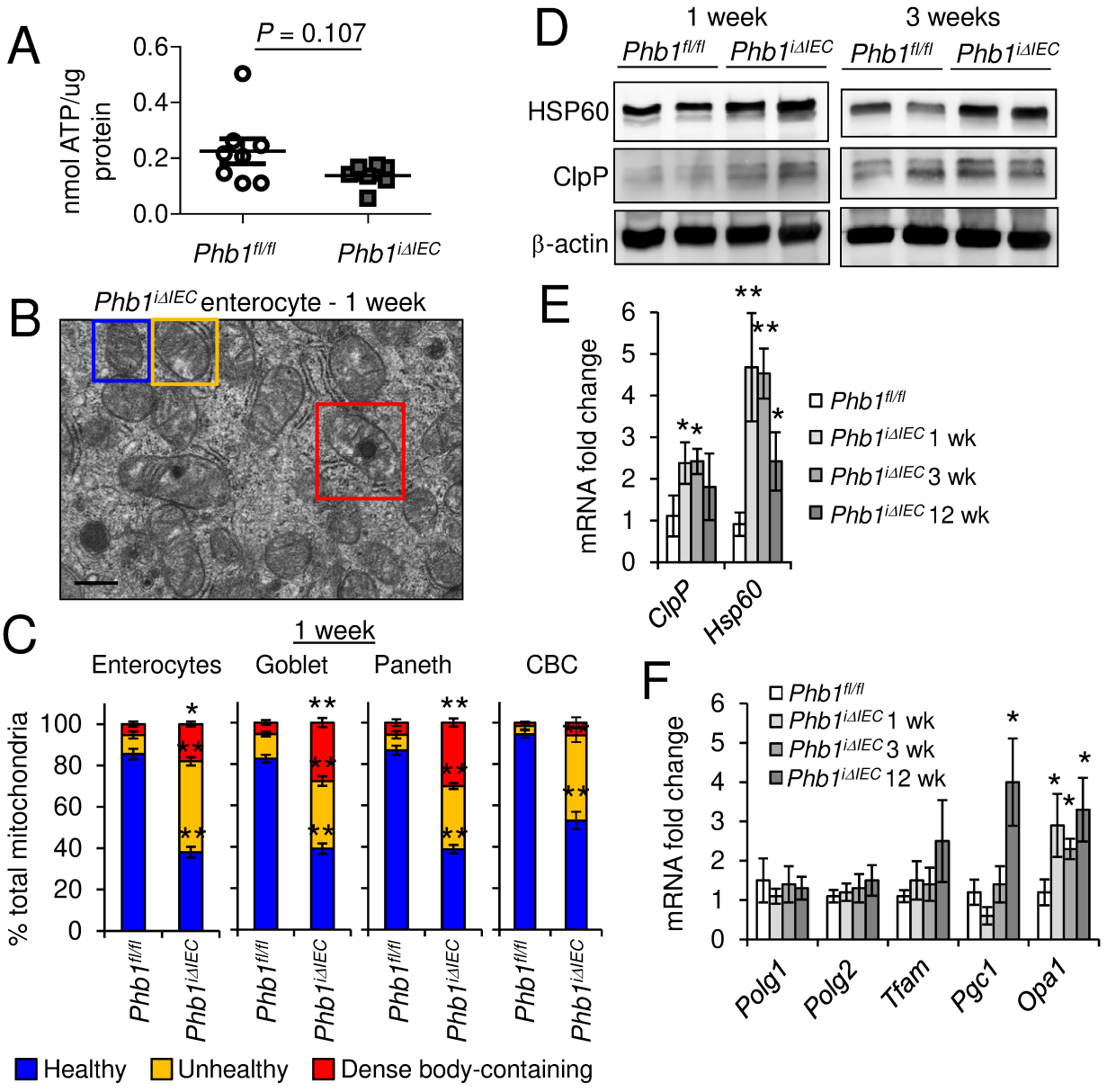

Fig. S6. *Phb1*$^{i\Delta IEC}$ ileal IECs exhibit mitochondrial dysfunction as early as 1 week after *Phb1* deletion. (**A**) ATP concentration in isolated ileal IECs 12 weeks after *Phb1* deletion. (**B**) TEM of ileal enterocyte. Representative healthy (blue box), unhealthy (yellow box), and dense inclusion body-containing (red box) mitochondria. Scale bar: 500 nm. (**C**) % healthy, unhealthy, and dense inclusion body-containing mitochondria visualized by TEM 1 week after PHB1 deletion. n = 200 enterocytes, 200 goblet cells, 50 Paneth cells, and 50 CBC cells with an average of 45 mitochondria/cell. (**D**) Representative western blots of mtUPR markers in isolated ileal IECs 1 or 3 weeks after PHB1 deletion. (**E-F**) mRNA expression of mtUPR markers (**E**) or genes controlling mitochondrial function (**F**) in isolated ileal IECs measured by qPCR. *Polg1* and *Polg2* maintain mtDNA copy number, *Tfam* regulates mtDNA transcription and replication, *Pgc1* is a master regulator of mitochondrial biogenesis, and *Opa1* regulates mitochondrial fusion, cristae remodeling, and bioenergetics. Results are presented as individual data points ± SEM (**A**) or as pooled data means ± SEM (**C**, **E**, **F**) of 8 mice (**A**, **D**), 4 mice (**C**), or 7 mice (**E**, **F**) per group. **P* < 0.05, ***P* < 0.01 by 1-way ANOVA followed by Bonferroni's test.

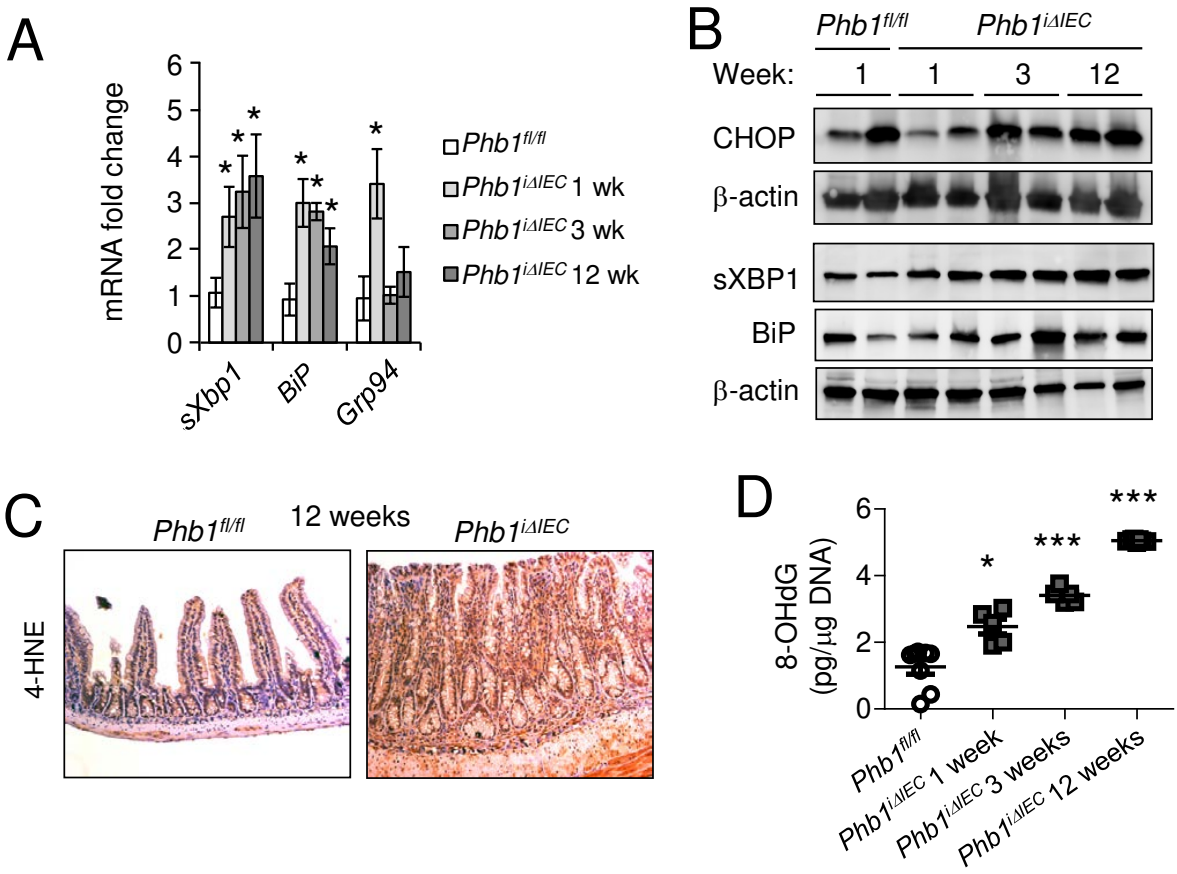

Fig. S7. Mitochondrial dysfunction in *Phb1*$^{i\Delta IEC}$ ileal IECs is accompanied with ER stress and oxidative stress. (**A**) mRNA expression of ER UPR markers in isolated ileal IECs 1, 3, or 12 weeks after PHB1 deletion measured by qPCR. (**B**) Representative western blots of CHOP, which is activated by both mtUPR and ER UPR to induce apoptosis, and mediators of ER UPR in isolated ileal IECs. (**C**) 4-HNE (marker of lipid peroxidation) IHC in ileum 12 weeks after *Phb1* deletion. (**D**) Ileum 8-OHdG (marker of oxidative damage of DNA) by ELISA. Results are presented as pooled data means ± SEM (**A**) or as individual data points ± SEM (**D**) of 7 mice (**A**) or 8 *Phb1*$^{fl/fl}$ and 6 *Phb1*$^{i\Delta IEC}$ mice (**B**, **D**) per group. **P* < 0.05, ****P* < 0.001 by 1-way ANOVA followed by Bonferroni's test.

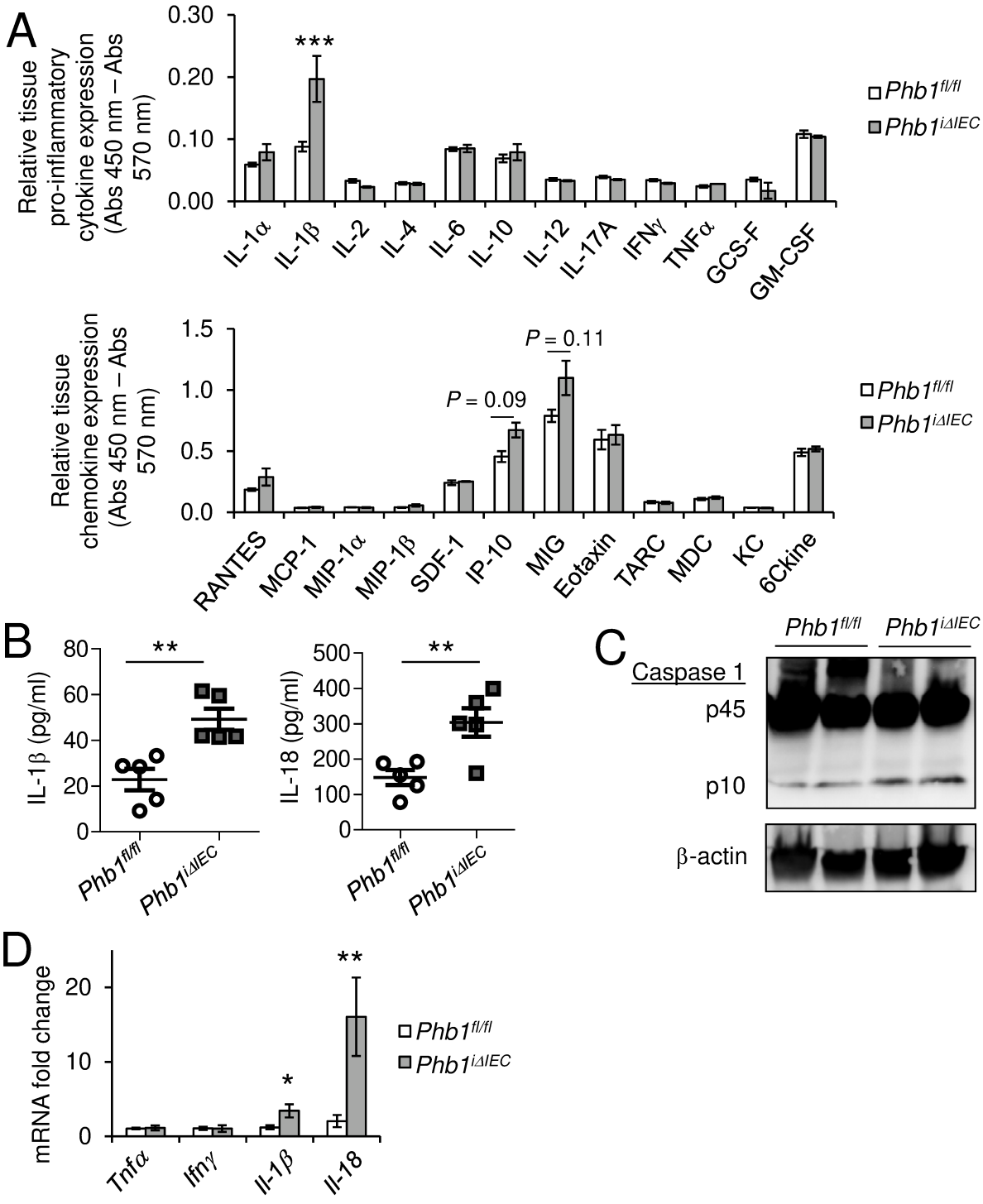

Fig. S8. IL-1β and IL-18 are increased in ileum of *Phb1*$^{i\Delta IEC}$ mice 1 week after *Phb1* deletion. (**A**) Multi-Analyte Elisa relative proinflammatory cytokine and chemokine expression. (**B**) Ileal IL-1β and IL-18 concentration by Elisa. (**C**) Representative western blots showing activated, cleaved form of Caspase 1 (p10) and procaspase 1 (p45). (**D**) Ileum mRNA expression measured by qPCR. Results are presented as pooled data means ± SEM (**A**, **D**) or individual data points ± SEM (B) of 3 mice (**A**) or 5 mice (**B**, **C**, **D**) per group. *P < 0.05, **P < 0.01, ***P < 0.001 by unpaired, 2-tailed Student's t test.

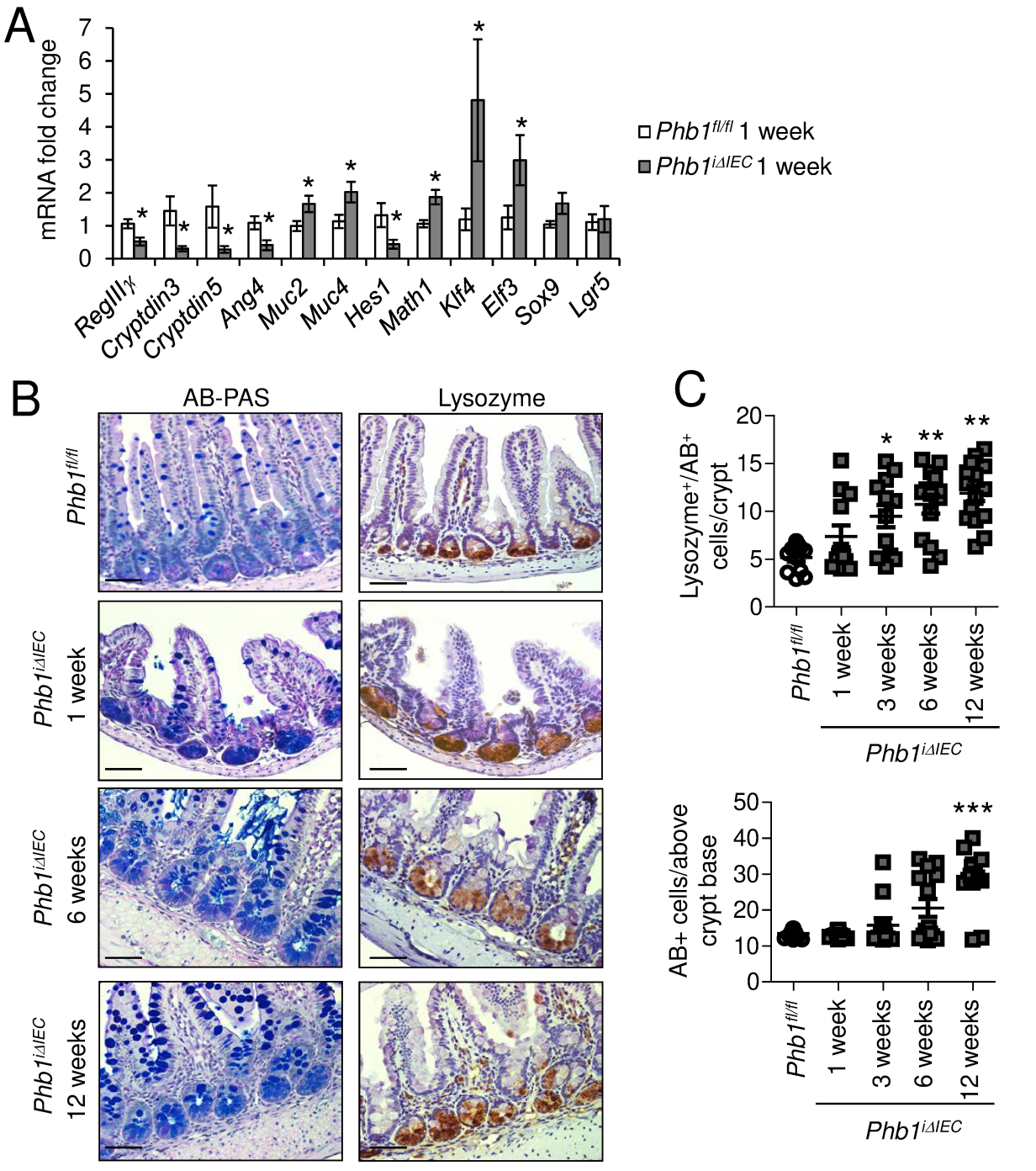

Fig. S9. *Phb1*$^{i\Delta IEC}$ mice exhibit intermediate cells earlier than increased goblet cells. (**A**) mRNA expression in ileal IECs 1 week after *Phb1* deletion measured by qPCR. (**B**) AB-PAS and Lysozyme stained sections. Scale bars: 250 μm. (**C**) The number of Lysozyme$^+$/Alcian blue$^+$ cells across 50 crypts per mouse. The number of Alcian blue$^+$ cells across 50 villi per mouse. Data are representative of 2 independent experiments. Results are presented as individual data points ± SEM (**A**) or as pooled data means ± SEM (**C**) of 8 mice per group (**A**) or 12 *Phb1*$^{fl/fl}$ mice and 12, 12, 14, or 15 *Phb1*$^{i\Delta IEC}$ mice at 1, 3, 6, or 12 weeks, respectively (**C**). *$P < 0.05$, **$P < 0.01$, ***$P < 0.001$ vs. *Phb1*$^{fl/fl}$ by 1-way ANOVA followed by Bonferroni's test.

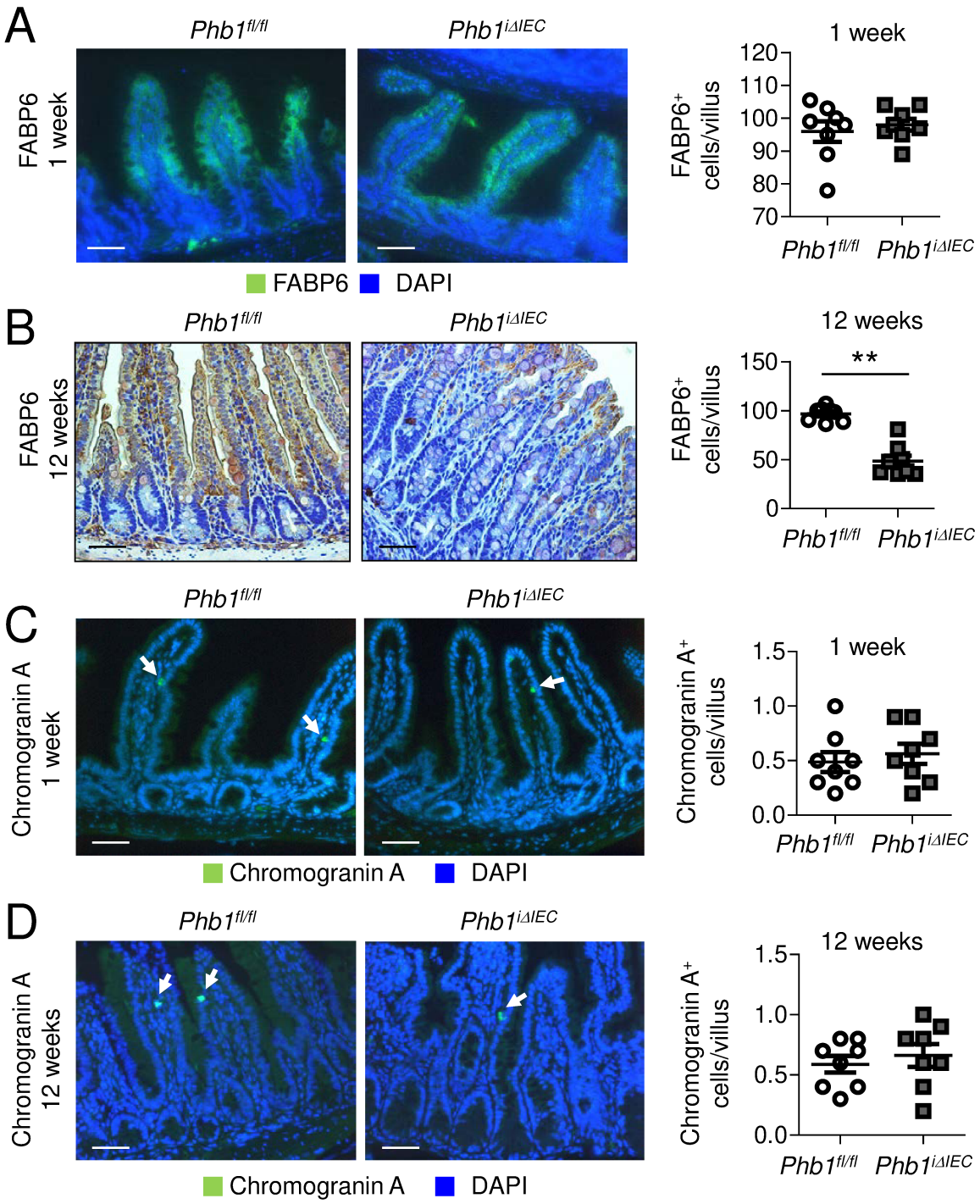

Fig. S10. Enterocyte numbers are decreased 12 weeks after *Phb1* deletion. (**A**) Fabp6 (enterocyte marker) immunofluorescent staining 1 week after *Phb1* deletion and quantitation of Fabp6$^+$ cells across 50 villi per mouse. (**B**) FABP6 IHC staining 12 weeks after *Phb1* deletion and quantitation of Fabp6$^+$ cells across 50 villi per mouse. Chromogranin A (enteroendocrine marker) immunofluorescent staining (arrows) 1 week (**C**) or 12 weeks (**D**) after *Phb1* deletion and quantitation of Chromogranin A$^+$ cells across 50 villi per mouse. Scale bars: 250 μm. Results are presented as individual data points ± SEM of 8 mice per group. $^{**}P < 0.01$ by unpaired, 2-tailed Student's t test.

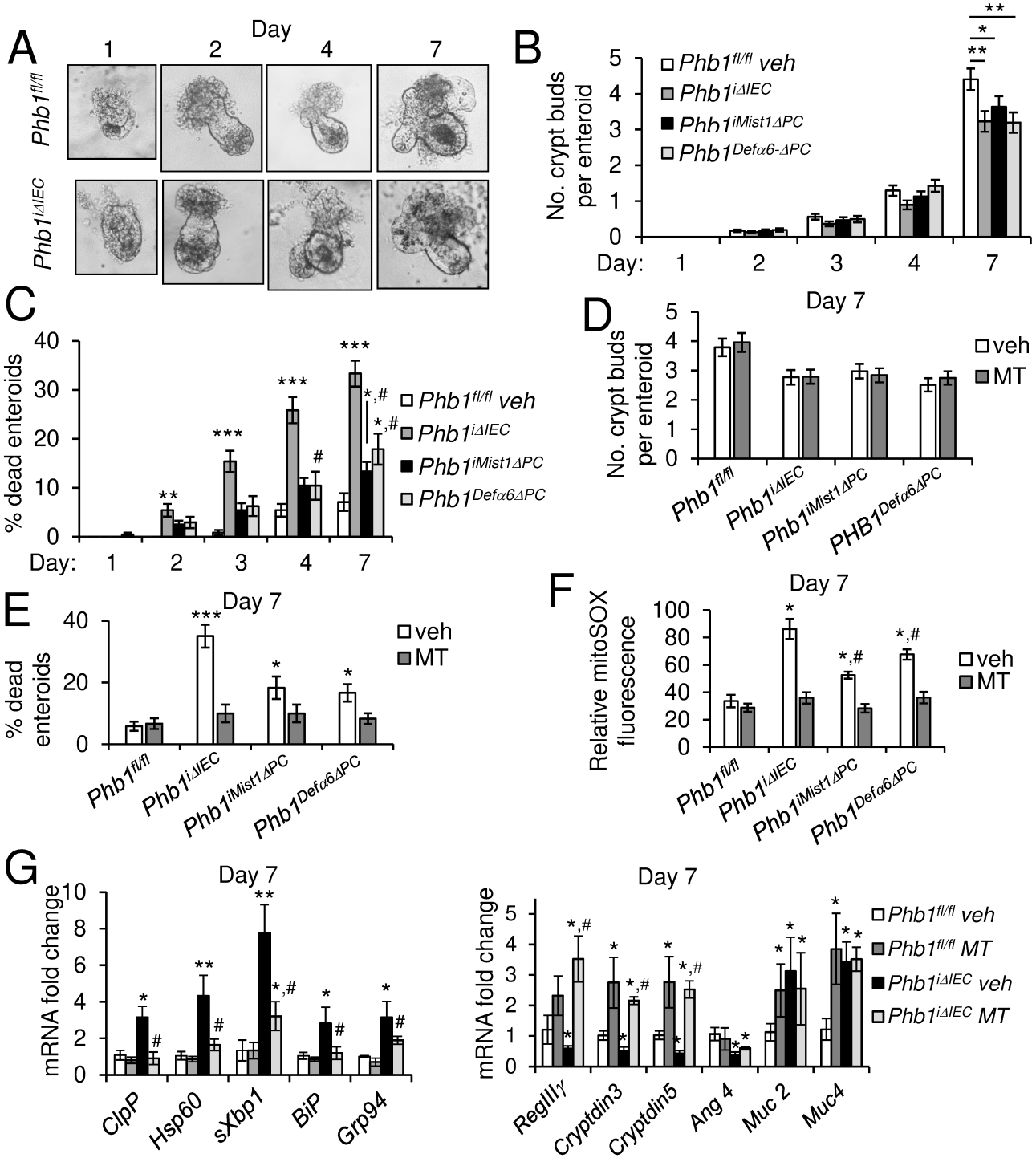

Fig. S11. *Phb1*-deficient enteroids exhibit decreased growth and viability that can be ameliorated by Mito-TEMPO (MT). (**A**) Phase-contrast images of cultured mouse ileal crypts in matrigel. (**B**) Number of crypt buds. (C) % dead enteroids. (**D**-**G**) Ileal enteroids were cultured in the presence of 25 nM MT or vehicle (veh). Number of crypt buds (**D**), % dead enteroids (**E**), mitoSOX (**F**), and mRNA expression was quantitated on day 7. Results are presented as pooled data means ± SEM of 20 wells with 10 enteroids/well per group (**B**-**F**) or 3 per group (**G**) . **P* < 0.05, ***P* < 0.01, ****P* < 0.01 vs. *Phb1*$^{fl/fl}$ veh, $^{\#}P$ < 0.05 vs. *Phb1*$^{i\Delta IEC}$ veh by 1-way ANOVA followed by Bonferroni's test.

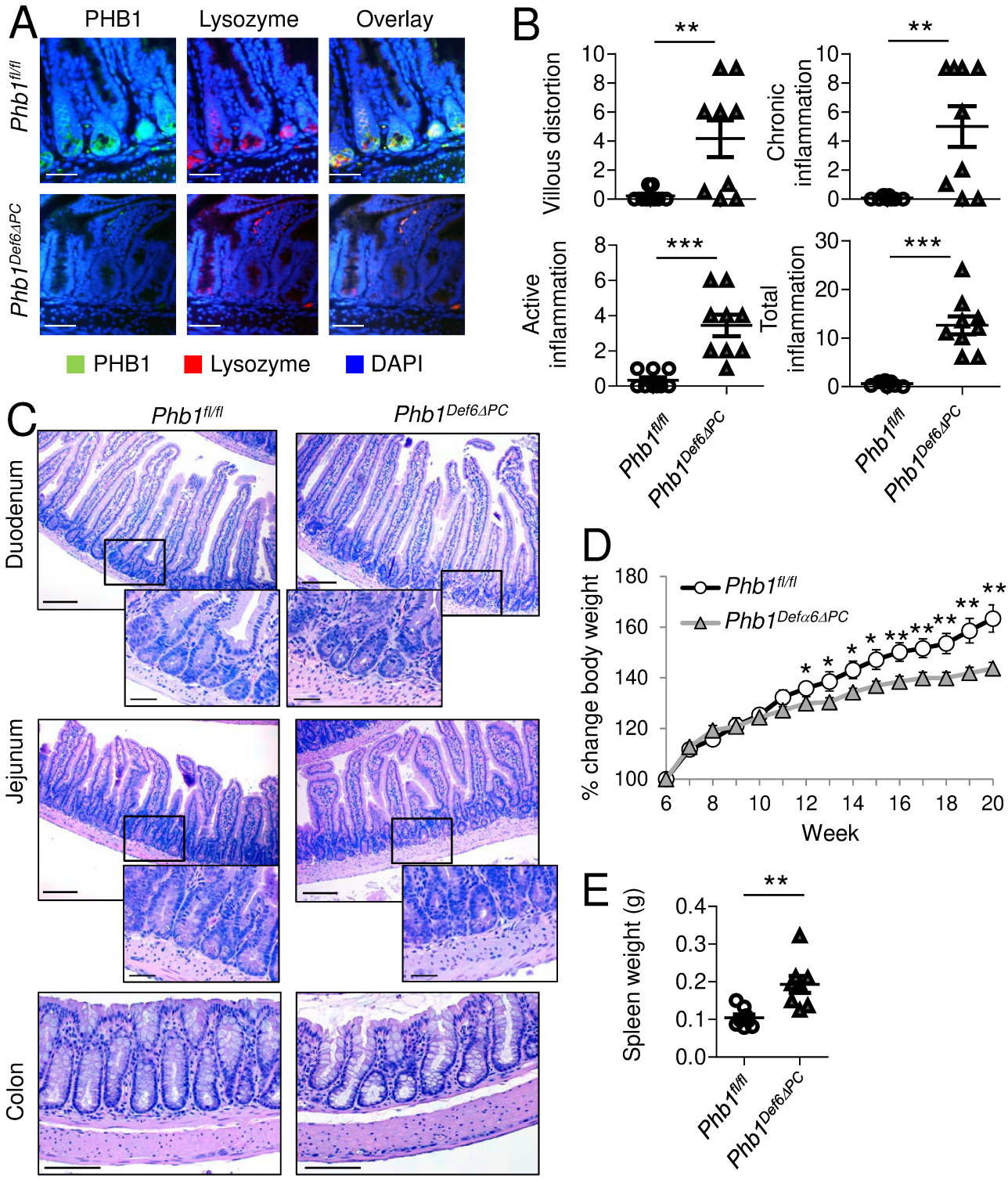

Fig. S12. *Phb1*$^{Def\alpha6\Delta PC}$ mice develop spontaneous ileitis. (**A**) PHB1 immunofluorescence staining. Scale bars: 125 μm. (**B**) Histological scoring of ileum by a blinded GI pathologist at 20 weeks of age. (**C**) Histology of duodenum, jejunum, and colon at 20 weeks of age. Scale bars: 250 μm, boxed pullouts: 75 μm. (**D**) % change body weight. (**E**) Spleen weight at 20 weeks of age. Results are presented as individual data points ± SEM (**B**, E) or as pooled data means ± SEM (**D**) of 9 mice per group. **P* < 0.05 ***P* < 0.01 ****P* < 0.001 by unpaired, 2-tailed Student's t test (**B**, **E**) or by 1-way ANOVA followed by Bonferroni's test (**D**).

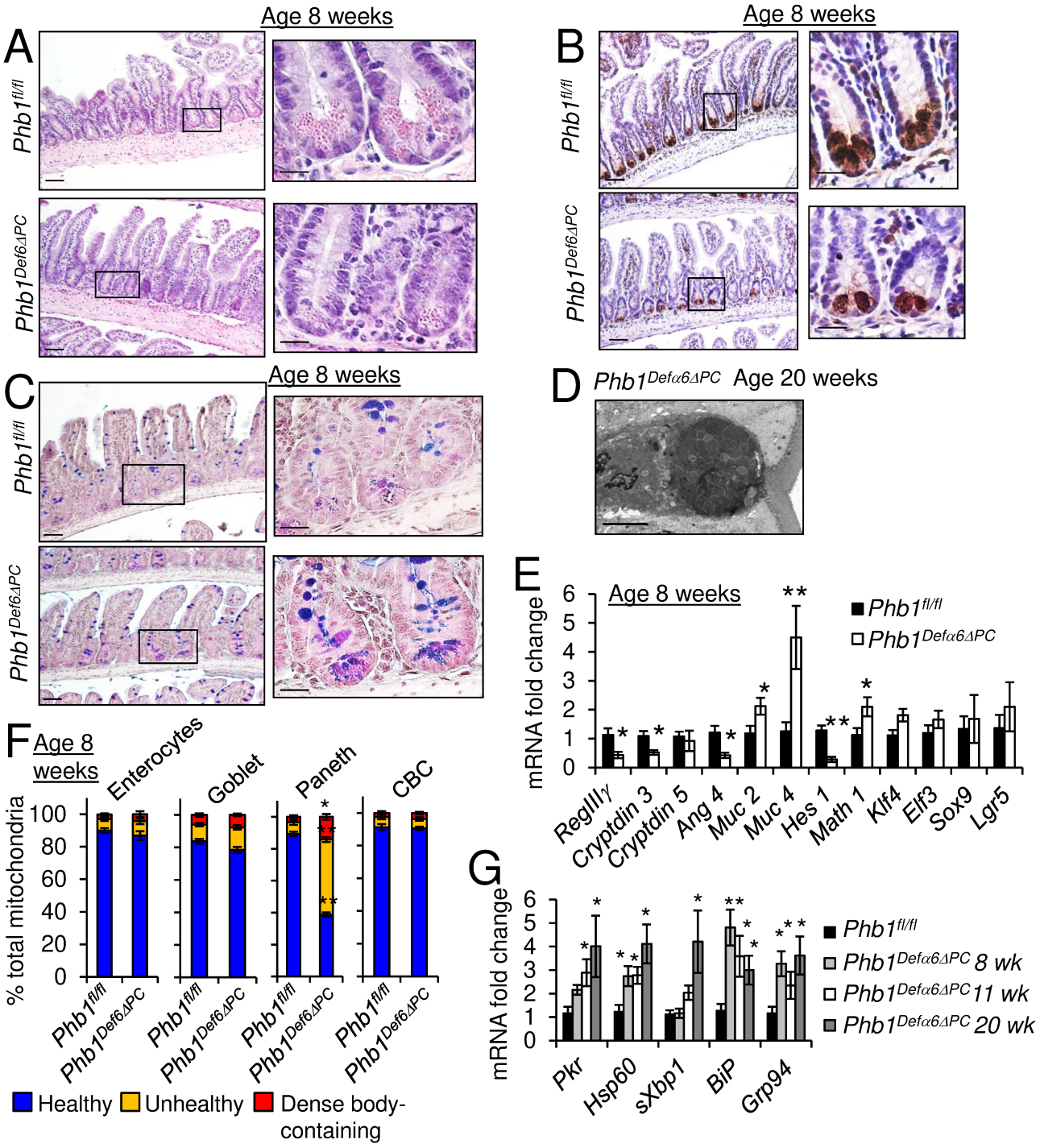

Fig. S13. *Phb1*^{Defα6ΔPC} mice exhibit Paneth cell defects as early as 8 weeks of age. (**A**) H&E staining. (**B**) Lysozyme immunohistochemistry. (**C**) AB-PAS staining. (**A**-**C**) Scale bars: 250 μm, boxed pullouts: 50 μm. (**D**) TEM of normal looking villus goblet cell. N, nucleus. Scale bar: 4 μm. (**E**) mRNA expression in isolated ileal IECs. (**F**) % healthy, unhealthy (swollen, dissolution of cristae), and dense inclusion body-containing mitochondria visualized by TEM. n = 200 enterocytes, 200 goblet cells, 50 Paneth cells, and 50 CBC cells. (**G**) mRNA expression in isolated ileal IECs. Results are presented as pooled data means ± SEM of 9 (**E**, **G**) or 4 (**F**) mice per group. **P* < 0.05 ***P* < 0.01 by 1-way ANOVA followed by Bonferroni's test.

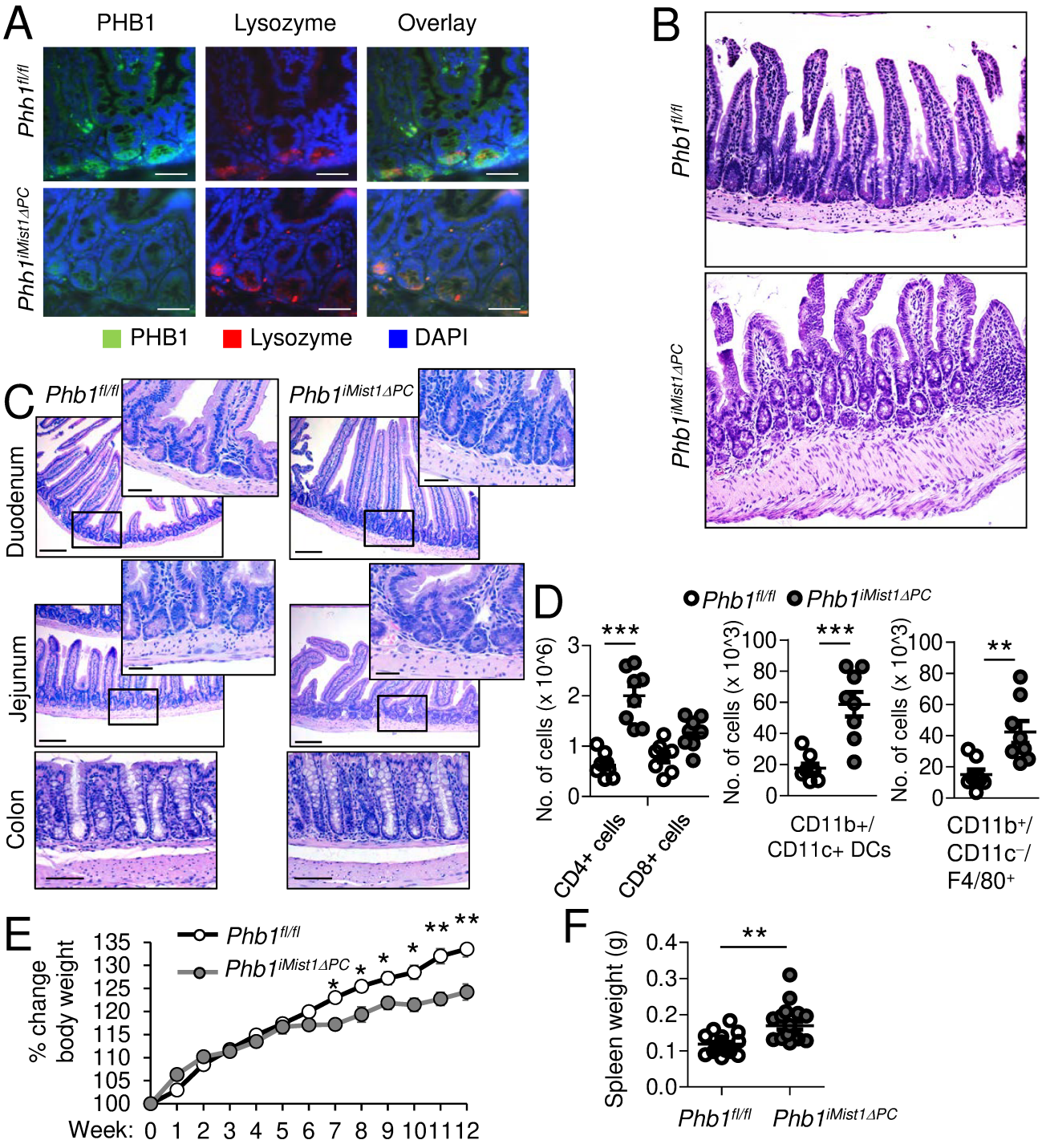

Fig. S14. *Phb1*$^{iMist1\Delta PC}$ mice develop spontaneous ileitis. (**A**) PHB1 immunofluorescence staining. Scale bars: 125 μm. (**B**-**F**) Time point shown is 12 weeks after the induction of *Phb1* deletion. (**B**) H&E-stained ileum. (**C**) Histology of duodenum, jejunum, and colon. Scale bars: 250 μm, boxed pullouts: 75 μm. (**D**) Absolute number of ileal LP immune cells calculated of total ileal LP cells. Data are representative of 2 independent experiments. (**E**) % change body weight after the induction of PHB1 deletion. (**F**) Spleen weight. Results are presented as individual data points ± SEM (**D**, **F**) or pooled data means ± SEM (**E**) of 8 (**D**) or 19 (**E, F**) mice per group. *$P < 0.05$ **$P < 0.01$ ***$P < 0.001$ by unpaired, 2-tailed Student's t test (**D**, **F**) or by 1-way ANOVA followed by Bonferroni's test (**E**).

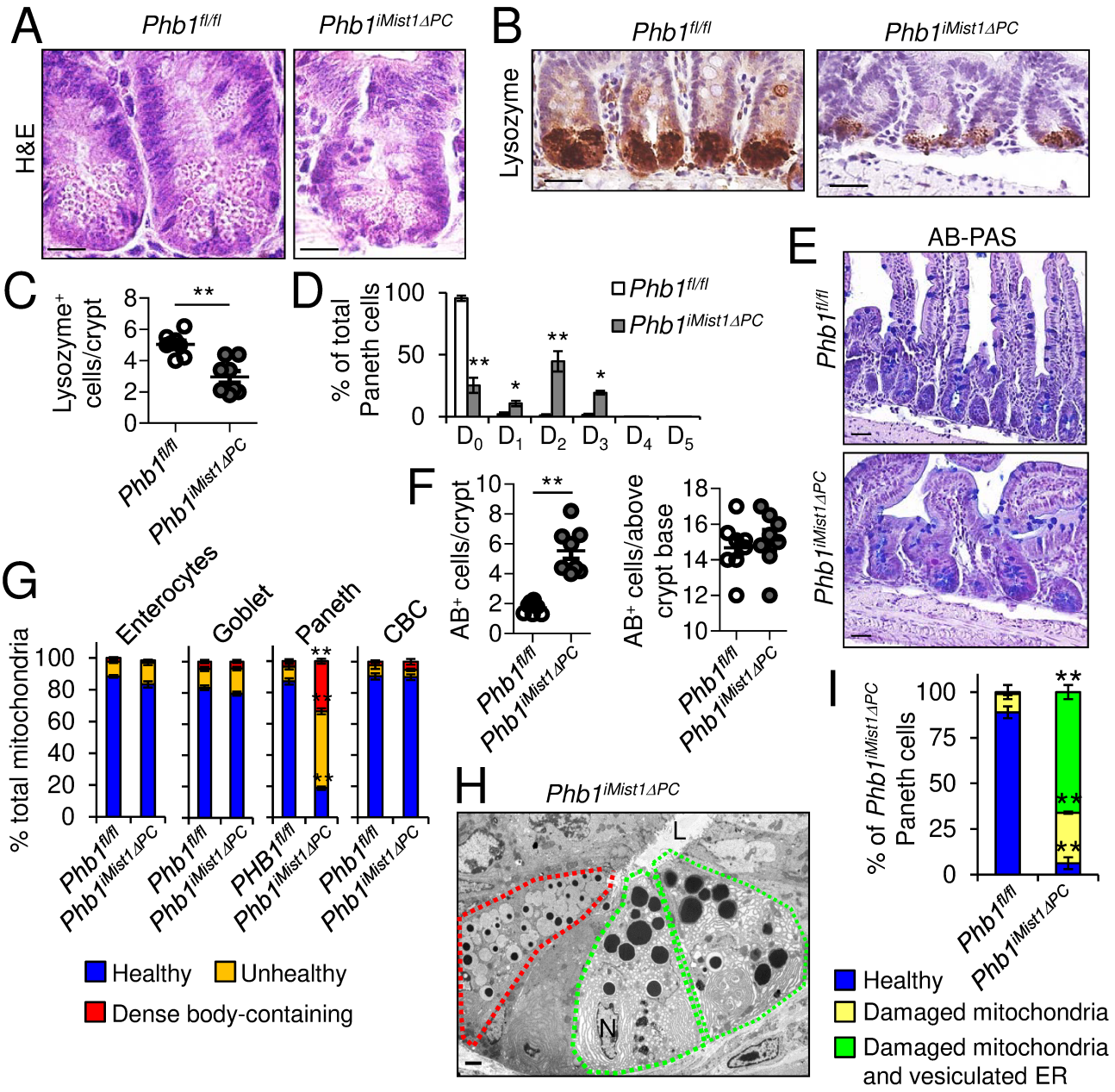

Fig. S15. *Phb1*$^{iMist1\Delta PC}$ mice exhibit Paneth cell abnormalities and mitochondrial dysfunction 1 week after *Phb1* deletion. (**A**) H&E-stained ileum. Scale bars: 50 μm. (**B**) Lysozyme IHC. Scale bars: 100 μm. (**C**) Lysozyme$^+$ cells/crypt. (**D**) Lysozyme staining pattern. (**E**) AB-PAS staining. Scale bars: 250 μm. (**F**) AB$^+$ cells. (**G**) % healthy, unhealthy (swollen, dissolution of cristae), and dense inclusion body-containing mitochondria visualized by TEM. n = 200 enterocytes, 200 goblet cells, 50 Paneth cells, and 50 CBC cells. (**H**) TEM of ileum crypt base. Goblet-like cell, red outline; Paneth cells with vesiculated ER, green outline. N, nucleus; L, lumen. Scale bar: 1 μm. (**I**) % of Paneth cells displaying vesiculated ER. Results are presented as individual data points ± SEM (**C**, **F**) or pooled data means ± SEM (**D**, **G**, **I**) of 8 (**C**, **D**, **F**) or 4 (**G**, **I**) mice per group. **P* < 0.05 ***P* < 0.01 by unpaired, 2-tailed Student's t test (C, F) or by 1-way ANOVA followed by Bonferroni's test (**D**, **G**, **I**).

Table S1. Proportion of *Phb1*$^{Def\alpha6\Delta PC}$ and *Phb1*$^{iMist1\Delta PC}$ mice that exhibit mitochondrial dysfunction, abnormal Paneth cells, and histological inflammation.

Age (weeks)	Week after *Phb1* deletion	% mice with mitochondrial dysfunction* n (%)		% mice with abnormal Paneth cells# n (%)		% mice with histological inflammation n (%)	
Phb1$^{Def\alpha6\Delta PC}$	*Phb1*$^{iMist1\Delta PC}$	*Phb1*$^{Def\alpha6\Delta PC}$	*Phb1*$^{iMist1\Delta PC}$	*Phb1*$^{Def\alpha6\Delta PC}$	*Phb1*$^{iMist1\Delta PC}$	*Phb1*$^{Def\alpha6\Delta PC}$	*Phb1*$^{iMist1\Delta PC}$
8	1	12/12 (100)	8/8 (100)	9/12 (75)	4/8 (50)	0/12 (0)	1/8 (13)
11	3	8/8 (100)	9/9 (100)	8/8 (100)	9/9 (100)	3/8 (38)	1/9 (11)
20	12	10/10 (100)	17/17 (100)	10/10 (100)	17/17 (100)	6/10 (60)	11/17 (65)

*Defined as increased mtUPR, ultrastructural abnormalities in IECs by TEM

#Defined as altered lysozyme staining, less abundant secretory granules, and AB^{+} staining.

Table S2. Quantitative real-time PCR primer sequences.

Primer name	Primer sequence
β-actin sense	5′-TATGCCAACACAGTGCTGTCTGG-3′
β-actin antisense	5′-TACTCCTGCTTGCTGATCCACAT-3′
Tnfα sense	5′-AGGCTGCCCCGACTACGT-3′
Tnfα antisense	5′-ACTTTCTCCTGGTATGAGATAGCAAA-3′
Il-1β sense	5′-TCGCTCAGGGTCACAAGAAA-3′
Il-1β antisense	5′-CATCAGAGGCAAGGAGGAAAAC-3′
Ifnγ sense	5′-CAGCAACAGCAAGGCGAAA-3′
Ifnγ antisense	5′-CTGGACCTGTGGGTTGTTGAC-3′
Il-10 sense	5′-GGTTGCCAAGCCTTATCGGA-3′
Il-10 antisense	5′-ACCTGCTCCACTGCCTTGCT-3′
Il-18 sense	5′-ACAACTTTGGCCGACTTCAC-3′
Il-18 antisense	5′-GGGTTCACTGGCACTTTGAT-3′
Reg3γ sense	5′-GCTTCCCCGTATAACCATCA-3′
Reg3γ antisense	5′-CCTTGCACCTGAGAAAGGAG-3′
Cryptdin 3 sense	5′-CCAGGCTGATCCTATCCAAA-3′
Cryptdin 3 antisense	5′-GACACAGCCTGGTCGTCTTC-3′
Cryptdin 5 sense	5′-GGCTGCAAAAGAAGAGAACG-3′
Cryptdin 5 antisense	5′-CAGCTGCAGCAGAATACGAA-3′
Ang4 sense	5′-GAGCCCATGTCCTTTGTTGT-3′
Ang4 antisense	5′-GCTTGGCATCATAGTGCTGA-3′
Muc2 sense	5′-ACATCACCTGTCCCGACTTC-3′
Muc2 antisense	5′-GAGCAAGGGACTCTGGTCTG-3′
Muc4 sense	5′-CCAGCAGCAAATCTCAAACA-3′
Muc4 antisense	5′-TCGCCAGGAGAGTTTGTTCT-3′
Hes1 sense	5′-ACACCGGACAAACCAAAGAC-3′
Hes1 antisense	5′-ATGCCGGGAGCTATCTTTCT-3′
Math1 sense	5′-CAACGACAAGAAGCTGTCCA-3′
Math1 antisense	5′-ATTTTTGCAGGAAGCTGTGG-3′
Klf4 sense	5′-AAGCCAAAGAGGGGAAGAAG-3′
Klf4 antisense	5′-CTGTGTGAGTTCGCAGGTGT-3′
Elf3 sense	5′-TTCAACGCCATGTACAGCTC-3′
Elf3 antisense	5′-TCCCTTTGGGATCTTGTCTG-3′
Sox9 sense	5′-CTGAAGGGCTACGACTGGAC-3′
Sox9 antisense	5′-TACTGGTCTGCCAGCTTCCT-3′
Lgr5 sense	5′-CCACAGCAACAACATCAGGT-3′
Lgr5 antisense	5′-AACAAATTGGATGGGGTTGT-3′
ClpP sense	5′- CATCTGCACGTGGTGTGTTG-3′
ClpP antisense	5′- GGAATTGGGCAGTGAATGGC-3′
Hsp60 sense	5′-TCTTCAGGTTGTGGCA-3′
Hsp60 antisense	5′-CCCCTCTTCTCCAAAC-3′
sXbp1 sense	5′-CTGAGTCCGAATCAGGTGCAG-3′
sXbp1 antisense	5′-GTCCATGGGAAGATGTTCTGG-3′
Total *Xbp1* sense	5′-TGGCCGGGTCTGCTGAGTCCG-3′

Total *Xbp1* antisense	5′-GTCCATGGGAAGATGTTCTGG-3′
BiP sense	5′-TTCAGCCAATTATCAGCAAACTCT-3′
BiP antisense	5′-TTTTCTGATGTATCCTCTTCACCAGT-3′
Grp94 sense	5′-AAGAATGAAGGAAAAACAGGACAAAA-3′
Grp94 antisense	5′-CAAATGGAGAAGATTCCGCC-3′
Polg1 sense	5′-GGAGATGAAGAAGTCGCTGATG-3′
Polg1 antisense	5′-CTCCTGCAAATCCCATTCTAGG-3′
Polg2 sense	5′-TCCTTGCGTTCTGTCTGTAAG-3′
Polg2 antisense	5′-CTTTCTCTGGAGGCTCTTCTTC-3′
Tfam sense	5′-GGAGCTACCAGAAGCAGAAA-3′
Tfam antisense	5′-GACTTGGAGTTAGCTGCTCTT-3′
Pgc1 sense	5′-CTAGCCATGGATGGCCTATTT-3′
Pgc1 antisense	5′-GTCTCGACACGGAGAGTTAAAG-3′
Opa1 sense	5′-CTCCCGACACAAAGGAAACTAT-3′
Opa1 antisense	5′-AATACTGCGCTCAGCATCTAC-3′

Supplementary Materials

Supplementary Methods

Mouse generation. Phb1$^{fl/fl}$ mice on the C57Bl/6 genetic background were generated by flanking exons 4 and 5 of the *Phb1* alleles with *loxP* sites as previously described.[1] Cre-mediated excision of exons 4 and 5 generates a frame shift mutation and early STOP codon at amino acid 117, resulting in a truncated, non-functional PHB1 protein lacking the C-terminus from Leu85 to Gln272.[1] *Phb1$^{fl/fl}$* mice were crossed with either *Villin-Cre-ER^{T2}* mice (kindly provided by Dr. Sylvie Robine, Institut Curie-CNRS, Paris), *Defα6-Cre* mice (described previously[2]), or *Mist1-Cre-ER^{T2}* mice (described previously[3]) (all C57Bl/6). The resulting offspring were genotyped by PCR analysis of tail genomic DNA obtained at weaning for expression of the floxed *Phb1* allele and *Villin-Cre-ER^{T2}*, *Defα6-Cre*, or *Mist1-Cre-ER^{T2}* transgenes using primer sequences previously described.[1-4] Experiments were performed with age- and gender-matched littermate mice. All mice were grouped-housed in standard cages under SPF conditions and were allowed standard chow and tap water *ad libitum*. All experiments were approved by the Baylor Scott & White Research Institute Institutional Animal Care and Use Committee.

Reagents and Antibodies. The following antibodies were used for western immunoblotting: PHB1 (70R-5543, polyclonal, Fitzgerald), PHB2 (14085, E1Z5A, Cell Signaling), Keratin 17 (4543, D73C7, Cell Signaling), CD3 (4443, CD3-12, Cell Signaling), Vimentin (49636, V9, Cell Signaling), PKR (sc136038, 13, Santa Cruz), ClpP (sc271284, B-12, Santa Cruz), Hsp60 (sc136291, 24, Cell Signaling), PCNA (ab18197, polyclonal, Abcam), Cleaved Caspase 3 (9661, Asp175, Cell Signaling), Cleaved Caspase 1 (sc56036, 14F468, Santa Cruz), CHOP (2895, L63F7, Cell Signaling), sXBP1 (12782, D2C1F, Cell Signaling), BiP (3177, C50B12, Cell

Signaling), β-actin (A1978, AC-15, Sigma-Aldrich). Antibodies were validated by western blot using the respective recombinant protein as positive control. The following antibodies were used for immunostaining: PHB1 (70R-5543, polyclonal, Fitzgerald), Lysozyme (sc27956, polyclonal, Santa Cruz), Muc2 (ab134119, EPR6145, Abcam), Ki67 (ACK02, K-2, Leica), Fabp6 (sc23994, polyclonal, Santa Cruz), Chromogranin A (ab45179, polyclonal, Abcam), 4-HNE (ab46545, polyclonal, Abcam). Isotype controls were included to validate immunostaining. The following secondary antibodies were used: donkey anti-goat IgG (Rhodamine Red X AffiniPure F(ab')$_2$ Fragment, 705-296-147, polyclonal, Jackson Immuno), donkey anti-rabbit IgG (FITC AffiniPure F(ab')$_2$ Fragment, 711-096-152, polyclonal, Jackson Immuno), Horseradish peroxidase-labeled goat anti-rabbit IgG (111-036-003, polyclonal, Jackson Immuno).

Inducible deletion of Phb1 from intestinal epithelial cells. Tamoxifen (Sigma Aldrich, St. Louis, MO) was prepared as described previously.[4] 8-week old *Phb1*$^{i\Delta IEC}$ mice and *Phb1*$^{iMist1\Delta PC}$ male and female mice were i.p. injected with 100 µl of 10 mg/ml tamoxifen for 4 consecutive days to induce deletion of *Phb1*. Mice were sacrificed 1, 3, 6 or 12 weeks after initial tamoxifen injection. Tamoxifen injections were repeated every 3-4 weeks to ensure continuity of PHB1 deletion.[4] Body weight was measured weekly. Of the 85 *Phb1*$^{i\Delta IEC}$ mice studied, 77 survived to the experimental endpoint; 6 mice died between weeks 3-6, 2 mice between weeks 9-12.

Treatment of mice with Mito-TEMPO. Concurrent with tamoxifen injection, 8-week old mice were i.p. injected with 500 µg/kg body weight Mito-TEMPO (Enzo Life Sciences) or vehicle (sterile saline) daily for 3 weeks. A subset of mice were administered Mito-Tempo (500 µg/kg body weight every other day) for an additional 9 weeks to assess severity of ileitis by histology.

Histology and Alcian Blue Periodic Acid-Schiff staining. Whole stomach and cecum and Swiss-rolls of small intestine and colon were fixed in 10% formalin and embedded in paraffin. To assess histology, 5-μm sections were stained with H&E. The entire GI tract was examined by trained GI pathologists (W.L.N. and K.T.) for alterations to tissue structure or inflammation. Sections of ileum were histologically scored by trained GI pathologists (W.L.N. and K.T.) in a blinded fashion for severity of villous distortion, active inflammation, and chronic inflammation as previously described.[5] Sections were stained with Alcian Blue (AB; Sigma Aldrich) solution, pH 2.5, for 5 minutes and washed in running tap water for 5 minutes. Sections were then stained with Periodic Acid and Schiff's (PAS) reagent according to PAS kit (Sigma Aldrich) protocol and mounted using xylene-based mounting media. Area of cytoplasmic mucin/cell for AB^+ cells above the crypt base was measured using Image J software (National Institutes of Health).

Transmission electron microscopy. Distal ileum was fixed in 2% gluteraldehyde in PBS, dehydrated and embedded in epoxy resin for electron microscopy. Ultrathin 70 nm sections were examined on a transmission electron microscope (Hitachi BioMedical TEM).

Immunohistochemistry. 7 μM paraffin-embedded sections of ileum were dehydrated in xylene and ethyl alcohol gradient, incubated in 0.3% H_2O_2 for 30 min, washed, incubated in 10mM sodium citrate for antigen epitope retrieval, blocked in 5% normal goat serum, and exposed to the appropriate antibody at 4ºC overnight. Peroxidase-labeled anti-rabbit immunoglobulin G secondary antibody and ABC reagent were added using the peroxidase-conjugated avidin ABC kit (Vector Laboratories, Burlingame, CA). Sections were counterstained with hematoxylin to visualize histology.

Terminal deoxynucleotidyl transferase-mediated dUTP nick end labeling (TUNEL) staining.

Immunofluorescent TUNEL staining was performed to measure apoptosis from paraffin-embedded sections using the In Situ Cell Death Detection kit as described by the manufacturer (Roche, Indianapolis, IN). Nuclei were stained with 4, 6'diamidino-2-phenylindole (DAPI) to assess total cells per crypt.

Isolation of intestinal epithelial cells (IECs). IEC isolation was performed as previously described.[6]

Detection of mitochondrial Complex I, II and IV activities, ATP, and 8-OHdG. The activities of Complexes I, II, and IV were measured in whole cell lysates of freshly isolated IECs using Complex I, II, and IV Microplate Assay Kits (Abcam) according to the manufacturer's instructions. 50 μg of protein extracted from ileum IECs was used. The concentration of adenosine triphosphate (ATP) in isolated IECs was determined using the ENLIGHTEN ATP Assay Bioluminescence Detection kit (Promega) according to the manufacturer's protocol. To measure 8-OHdG, DNA was extracted (DNeasy Kit, Qiagen) from homogenized ileal samples, digested using nuclease P1 (New England Biolabs), and measured for 8-OHdG by ELISA (Abcam).

Flow cytometry. Mesenteric lymph nodes from the ileum were removed using a dissecting microscope. Lamina propria immune cells were isolated using the Mouse Lamina Propria Dissociation Kit (Miltenyi) and counted using the Countess II Automated Cell Counter. The following antibodies were used for flow cytometry (BD FACSAria III): violetFluor™ 450 Anti-Mouse CD45 (75-0451-U025, Tonbo), APC-Cyanine7 Anti-Mouse CD4 (25-0042, Tonbo), FITC Anti-Mouse TCR beta (35-5961, Tonbo), PE-Cyanine5 Anti-Human/Mouse CD11b (55-

0112, Tonbo), APC Anti-Mouse CD11c (20-0114-U025, Tonbo), PE-Cyanine7 Anti-Mouse F4/80 Antigen (60-4801, Tonbo), 7-AAC (13-6993, Tonbo).

Western blot analysis. Total protein was isolated from whole ileum or isolated IECs and separated by SDS-PAGE and analyzed by western blotting as described previously.[7]

Cytokine ELISA. Whole ileum was homogenized and analyzed using the Mouse Inflammatory Cytokines Multi-Analyte ELISArray Kit and the Mouse Common Chemokines Multi-Analyte ELISArray Kit (Qiagen) as described by the manufacturer. IL-1β and IL-18 were assayed using ELISA kits from Abcam.

RNA isolation and quantitative real-time PCR analysis. Total RNA was isolated from ileum using the RNeasy kit (Qiagen, Valencia, CA). Quantitative real-time PCR was performed as described previously.[7] For graphical representation of quantitative PCR data, the $\Delta\Delta C_T$ was calculated as follows: $\Delta\Delta C_T = (Ct,_{\text{target}} - Ct,_{\beta\text{-actin}})_{Phb1i\Delta IEC\ or\ Phb1\Delta PC} - (Ct,_{\text{target}} - Ct,_{\beta\text{-actin}})_{Phb1fl/fl}$, with the final graphical data derived from $2^{-\Delta\Delta CT}$. Primers sequences used for quantitative RT-PCR are provided in Supplemental Table 2.

16S rRNA gene sequencing. Stool was collected from $Phb1^{fl/fl}$ and $Phb1^{i\Delta IEC}$ F2 generation littermates at baseline prior to tamoxifen injection (week 0, two separate collections 1 day apart) and 1, 3, and 12 weeks after *Phb1* deletion. Mice were co-housed throughout the experiment to standardize the gut microbiota for isolating the contribution of genetics to phenotype.[8] DNA extraction, 16S ribosomal RNA gene PCR amplication, and sequencing on an Illumina MiSeq platform was performed by Diversigen, Houston, TX. MiSeq Reagent kit (v3) was used with 2 ×

300 bp read lengths. Mothur software was used to analyze α and β diversity of taxonomic classification and principle coordinates analysis.

Ileal enteroid culturing. Mouse ileal crypts were isolated and plated in Reduced Growth Factor Matrigel (356230, BD Biosciences) using the method by Sato et. al.[9] Enteroids were cultured in Advanced DMEM/F-12 (12634-010, Gibco, ThermoFisher) supplemented with GlutaMAX (Gibco 35050-061, ThermoFisher), Pen/Strep (P4458, Sigma Aldrich), HEPES (Gibco 15630-080, ThermoFisher), 1× N2 supplement (Gibco 17502-048, ThermoFisher), 1 ng/μl EGF (2028-EG, R&D Systems, Minneapolis, MN), 2 ng/μl Noggin (250-38, PeproTech, Rocky Hill, NJ), 10 ng/μl murine R-spondin (3474-RS-050, R&D Systems), and Y27632 (ALX-270-333-M025, Enzo Life Sciences, Farmingdale, NY). Enteroids were counted at day 1, and bud formation and death by visualizing altered morphology as described[10] were assessed at day 2, 3, 4, and 7 using an Zeiss Axioskope Plus Inverted Microscope. Enteroids were harvested at day 7 and RNA was isolated using RNeasy kits (Qiagen). 100 nM Mito-Tempo (Enzo Life Sciences) or vehicle were added daily with fresh media from days 0-7 of culture. MitoSOX fluorescence was measured on day 7 by incubating enteroids in with Hank's balanced salt solution (HBSS) with 5 μM MitoSOX Red Mitochondrial Superioxide Indicator dye (Invitrogen) for 10 min at 37°C. Enteroids were washed twice with warm HBSS and fluorescent intensity was measured at 510 nm excitation/580 nm emission. Fluorescent intensity was normalized to number of enteroids.

Statistical analysis. Values are expressed as mean ± SEM or as individual data points ± SEM. Statistical analysis was performed using unpaired 2-tailed Student's *t* test was used for single comparisons and 1-way ANOVA with Bonferroni post-hoc test for multiple comparisons (PRISM 6.0, GraphPad Software). For experiments using Mito-TEMPO treatment, statistical

analysis was performing using 2-way ANOVA and subsequent Bonferroni post-hoc tests. $P < 0.05$ was considered significant.

Patient and public involvement. Patients/the public were not involved in the design of this study.

Supplementary Materials References

1. He B, Kim TH, Kommagani R*, et al.* Estrogen-regulated prohibitin is required for mouse uterine development and adult function. *Endocrinology* 2011;**152**, 1047-1056.
2. Adolph TE, Tomczak MF, Niederreiter L*, et al.* Paneth cells as a site of origin for intestinal inflammation. *Nature* 2013;**503**, 272-276.
3. Shi G, Zhu L, Sun Y*, et al.* Loss of the acinar-restricted transcription factor Mist1 accelerates Kras-induced pancreatic intraepithelial neoplasia. *Gastroenterology* 2009;**136**, 1368-1378.
4. el Marjou F, Janssen KP, Chang BH*, et al.* Tissue-specific and inducible Cre-mediated recombination in the gut epithelium. *Genesis* 2004;**39**, 186-193.
5. Burns RC, Rivera-Nieves J, Moskaluk CA*, et al.* Antibody blockade of ICAM-1 and VCAM-1 ameliorates inflammation in the SAMP-1/Yit adoptive transfer model of Crohn's disease in mice. *Gastroenterology* 2001;**121**, 1428-1436.
6. Nenci A, Becker C, Wullaert A*, et al.* Epithelial NEMO links innate immunity to chronic intestinal inflammation. *Nature* 2007;**446**, 557-561.
7. Theiss AL, Vijay-Kumar M, Obertone TS*, et al.* Prohibitin is a novel regulator of antioxidant response that attenuates colonic inflammation in mice. *Gastroenterology* 2009;**137**, 199-208, 208 e191-196.
8. Robertson SJ, Lemire P, Maughan H*, et al.* Comparison of Co-housing and Littermate Methods for Microbiota Standardization in Mouse Models. *Cell Rep* 2019;**27**, 1910-1919 e1912.
9. Sato T, Vries RG, Snippert HJ*, et al.* Single Lgr5 stem cells build crypt-villus structures in vitro without a mesenchymal niche. *Nature* 2009;**459**, 262-265.
10. Grabinger T, Luks L, Kostadinova F*, et al.* Ex vivo culture of intestinal crypt organoids as a model system for assessing cell death induction in intestinal epithelial cells and enteropathy. *Cell Death Dis* 2014;**5**, e1228.